Title: Studies of styrene oxidation by catalyst based on Zeolite-Y nanohybrid materials

Author: Nisheeth C. Desai Jiten A. Chudasama Tushar J. Karkar Bonny Y. Patel Krunalsinh A. Jadeja Dinesh R. Godhani Jignasu P. Mehta

PII: S1381-1169(16)30366-1
DOI: http://dx.doi.org/doi:10.1016/j.molcata.2016.08.031
Reference: MOLCAA 10018

To appear in: *Journal of Molecular Catalysis A: Chemical*

Received date: 21-7-2016
Revised date: 19-8-2016
Accepted date: 29-8-2016

Please cite this article as: Nisheeth C.Desai, Jiten A.Chudasama, Tushar J.Karkar, Bonny Y.Patel, Krunalsinh A.Jadeja, Dinesh R.Godhani, Jignasu P.Mehta, Studies of styrene oxidation by catalyst based on Zeolite-Y nanohybrid materials, Journal of Molecular Catalysis A: Chemical http://dx.doi.org/10.1016/j.molcata.2016.08.031

Graphical abstract

Studies of styrene oxidation by catalyst based on Zeolite-Y nanohybrid materials

Nisheeth C. Desai*, Jiten A. Chudasama, Tushar J. Karkar, Bonny Y. Patel, Krunalsinh A. Jadeja, Dinesh R. Godhani and Jignasu P. Mehta

Department of Chemistry (UGC NON-SAP & DST-FIST Sponsored), Mahatma Gandhi Campus, Maharaja Krishnakumarsinhji Bhavnagar University, Bhavnagar 364 002, India
E-mail: *dnisheeth@rediffmail.com*

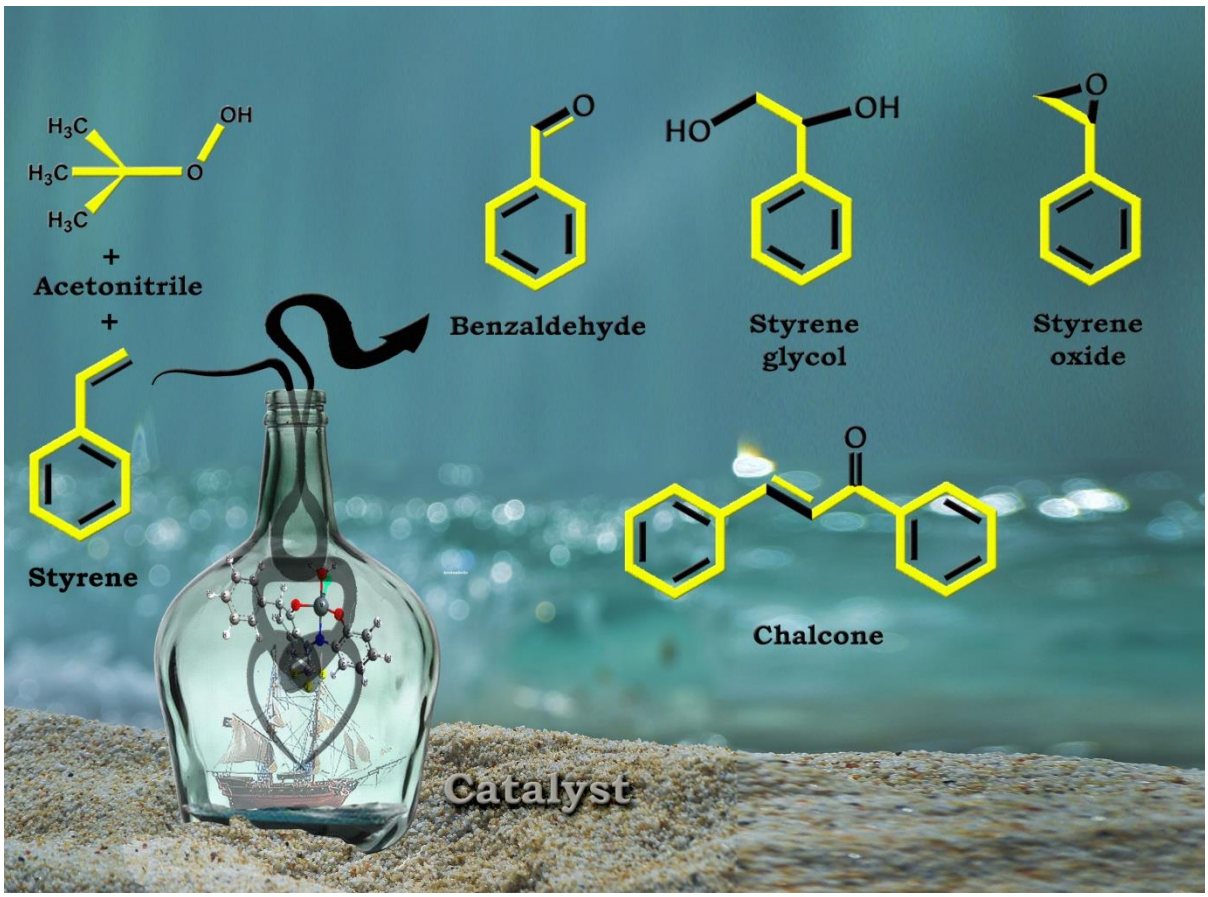

Studies of styrene oxidation by catalyst based on Zeolite-Y nanohybrid materials

Nisheeth C. Desai*, Jiten A. Chudasama, Tushar J. Karkar, Bonny Y. Patel, Krunalsinh A. Jadeja, Dinesh R. Godhani and Jignasu P. Mehta

Department of Chemistry (UGC NON-SAP & DST-FIST Sponsored), Mahatma Gandhi Campus, Maharaja Krishnakumarsinhji Bhavnagar University, Bhavnagar 364 002, India

E-mail: *dnisheeth@rediffmail.com*

Highlights

- We have combined VO(IV) based neat and their entrapped complexes into the nanopores of zeolite-Y.
- The comparative studies of spectroscopic, thermal, morphological and crystalline properties of complexes were achieved.
- The catalytic activities were tried over oxidation of styrene reaction using TBHP as an oxidizing agent.
- The reaction parameters were optimized for higher oxidation with higher selectivity towards allylic products.
- Among all catalysts, [VO(HNIMMPP)(H_2O)]-Y catalyst showed higher catalytic (TOF, 114.75 h^{-1}) activity with 45% selectivity of benzaldehyde.

ABSTRACT

Metal complexes of VO(IV), Mn(II), Fe(II), Co(II), Ni(II), Cu(II) and HNIMMPP (4-(((2-Hydroxy-5-nitrophenyl)imino)methyl)-3-methyl-1-phenyl-1*H*-pyrazol-5-ol) schiff base ligand have been synthesized within zeolite-Y along with neat one. Synthesized compounds were characterized by physico-chemical techniques such as elemental analysis of catalysts, BET, XRD, SEM, FT-IR, UV-Vis, ICP-OES and TGA. Synthesized zeolite-Y based nanohybrid materials and their uncovered complexes were used in styrene oxidation with TBHP as an oxidizing agent. Oxidation reaction of styrene furnished benzaldehyde as the major product and styrene glycol, chalcone and 2-phenyloxirane as minor products. Amongst all catalysts, [VO(HNIMMPP)(H_2O)]-Y produced the highest conversion at 93.35% and selectivity of benzaldehyde (45.70%) was the greatest. These nanohybrid materials can be easily reprocessed and recovered within these reaction parameters. The reaction mechanism for catalytically oxidized styrene is discussed in the present paper.

Keywords: Zeolite-Y; Nanohybrid materials; Styrene oxidation

1. Introduction

Oxy-functionalized derivatives of olefins are vital raw constituents for fine chemicals, pharmaceuticals, agrochemicals, and fragrance industry because they usually demonstrate interesting organoleptic properties [1-4]. Oxidation of olefins produces significant products like acids, aldehydes, epoxides, alcohols and ketones etc. These products are key ingredients in many chemical industries [5, 6]. Catalytic oxidation of olefins can be easily completed by metal complexes in homogeneous reaction media [7, 8]. Heterogeneous catalysis is a dynamic field of research for oxidation in many industrial reactions as compared to homogeneous catalyst [9, 10]. For the growth of novel chemical technologies, zeolite imprisoned metal complexes hold a significant place amongst heterogeneous catalysts [11, 12].

Several transition metal complexes (TMC) as homogeneous catalyst are crucial for various organic reactions. However these catalysts faced the problems of corrosion, contamination of products, reusability and difficulties in separation at the time of reaction accomplishment. To overcome these technical issues, the recent advancements in catalysis are mainly concentrated on entrapment of metal complexes either on inert or on porous solid materials [13-22]. These heterogeneous catalysts afford the following advantages to liquid phase reaction such as minimization of waste, recyclability and reprocessing from the reaction mixture [23-25]. Zeolite-Y imprisoned TMCs are more appropriate since they do not easily come out for the duration of the catalytic reaction after the complexation [26, 27].

Homogeneous as well as heterogeneous catalysts were used for the epoxidation of styrene [28-33]. Styrene oxidation furnished important products such as diols, carbonyl compounds, epoxides, and oxidative cleavage of C-C bond. With the advancement in homogeneous catalysis along with a heterogeneous catalyst as zeolite-Y imprisoned TMCs played a significant role to enhance the styrene oxidation [34-36].

In the present work our focus was based on nanohybrid catalytic studies related to zeolite-Y of VO(IV), Mn(II), Fe(II), Co(II), Ni(II), Cu(II) transition metal complexes and HNIMMPP Schiff base ligands. These heterogenic catalysts were used for oxidation of styrene with TBHP as oxidant and characterised by GCMS. For

the characterization of the synthesized compounds standard analytical techniques were used.

2. Experimental

2.1. Materials and reagents

AR grad chemicals were utilized without further refinement. $POCl_3$ (99%), DMF (99.5%) (Spectrochem, India), 1-phenyl-3-methyl-2-pyrazoline-5-one (99%) (Sigma-Aldrich, Germany) and 2-amino-4-nitro phenol (Sigma-Aldrich, Germany). $MnSO_4 \cdot H_2O$, $FeSO_4 \cdot 7H_2O$, $CoSO_4$, $NiSO_4 \cdot 6H_2O$, $CuSO_4 \cdot 5H_2O$ and $VOSO_4 \cdot 5H_2O$ were procured from Merck. Sodium form of zeolite-Y (Na-Y, By-600, mole ratio of SiO_2/Al_2O_3 5:2, nominal cation hydrogen, surface area = 660 m^2/g) was procured from Reliance, India. The catalytic activities of the prepared samples were monitored by substrates like (commercially obtained 70%) TBHP (Spectrochem, India) and styrene-99% (Sigma-Aldrich, Germany). Solvents such as acetone (99%), methanol (99%), ethanol (99.9%) and THF (99.5%) have been used. Compounds are characterized by standard analytical techniques and details were given in supplementary data.

2.2. Preparation of Schiff base

The Schiff base was prepared in two steps:

Step 1. Preparation of 1-Phenyl-3-methyl-4-formyl-1H-pyrazol-5-ol

1-Phenyl-3-methyl-4-formyl-1*H*-pyrazol-5-ol (PMFP) was prepared by the condensation reaction of 1-phenyl-3-methyl-1*H*-pyrazol-5-ol (PMP) in dimethylformamide and $POCl_3$ [24]. 1-Phenyl-3-methyl-1*H*-pyrazol-5-ol (8.7 g, 0.050 mol) in dimethylformamide (10.0 cm^3, 0.050 mol) was chilled to 0 °C in ice bath. Drop wise addition of phosphoryl chloride (5.50 cm^3, 0.060 mol) was performed to control the temperature between 10 to 20 °C. After completion of addition, the reaction mixture was heated on steam bath for 1.5 h and at that point transferred into ice water. Then it was allowed to stand overnight and product was filtrated, washed with water and dried. It was further crystallized using ethanol (99.9%). Yellow crystals of PMFP were obtained in 83% yield and m.p. 176 °C [37] (Fig. 1).

Step 2. Preparation of 4-(((2-Hydroxy-5-nitrophenyl)imino)methyl)-3-methyl-1-phenyl-1H-pyrazol-5-ol (HNIMMPP)

4-(((2-Hydroxy-5-nitrophenyl)imino)methyl)-3-methyl-1-phenyl-1*H*-pyrazol-5-ol (HNIMMPP) was prepared by condensation reaction of 1-phenyl-3-methyl-4-formyl-1*H*-pyrazol-5-ol (PMFP) and 2-amino-4-nitrophenol. They were mixed in a RBF containing 40 mL of THF and refluxed under water bath for 4-6 h. Filtered, dried and collected crude product was recrystallized in 1,4-dioxane (Fig. 2).

2.3. Preparation of transition metal complexes

TMCs were prepared by a condensation reaction between ligand (HNIMMPP) and respective metal salt. Prepare 1 mole of HNIMMPP solution in ethanol (95%) and 1 mole of metal salt ($MnSO_4 \cdot H_2O$, $FeSO_4 \cdot 7H_2O$, $CoSO_4$, $NiSO_4 \cdot 6H_2O$, $CuSO_4 \cdot 5H_2O$, and $VOSO_4 \cdot 5H_2O$) solution in distilled water, mix both of these solutions in RBF and refluxed for 4-6 h. The progress of reaction was monitored by TLC. The mixture was allowed to settle overnight then filtered and dried. The separated product was recrystallized by THF (Fig. 3).

2.4. Preparation of zeolite-Y imprisoned transition metal complexes

Flexible ligand method (FLM) was used to synthesize zeolite-Y imprisoned transition metal complexes. The stepwise method to imprison TMCs in inner side to the nanocavity of zeolite-Y is as shown below:

2.4.1. Synthesis of metal-exchanged zeolite-Y [M(II/IV)-Y]:

In this step of ion-exchange, alkali metal ion such sodium would be replaced by transition metal ion from the matrix of zeolite-Y. A quantity of 5 g of zeolite-Y (Na-Y) was taken in 300 mL of deionized water containing 12 mmol metal salts [For Mn(II), Fe(II), Co(II), Ni(II) Cu(II), and VO(IV): 2.49 g, 3.33 g, 2.98 g, 2.98 g, 2.39 g, and 3.13 g, respectively] through continuous stirring at 90 °C for 22 to 30 h. The solid M (II/IV)-Y was filtered, washed with hot deionized water till the filtrate was free from metal ion content and then dried for 15 h at 120 °C. The schematic diagram is shown in Fig. 4.

2.4.2. Synthesis of zeolite-Y imprisoned transition metal complexes:

1.0 g of M(II/IV)-Y was uniformly mixed with an excessive amount of Schiff base ligands (n_{ligand}/n_{metal} = 3) in THF. The mixture was heated (~24 h) in an oil-bath through continuous stirring. After crude material of novel catalyst was precipitated out, Soxhlet extraction method was utilized to remove the undesired part of raw materials and complex stuck on the outer surface of zeolite-Y with help of suitable solvents THF, acetone, ethanol and finally by acetonitrile (6-8 h). 0.01 M NaCl solution was used for ion-exchange of the extracted part for 22-24 h to eliminate uncoordinated metal ions and washed by deionized water till no chloride ions could be detected with $AgNO_3$ solution. The final material was collected and dried at 120 °C. The schematic diagram is shown in Fig. 4.

3. Results and discussion

3.1. Characterization of Zeolite-Y based nanohybrid materials

The elemental data of Schiff base ligand, neat complexes, zeolite-Y and its imprisoned TMCs are specified in Table 1. The elemental study of the imprisoned compounds revealed the existence of organic matter and central metal ions with C-N ratio equivalent to that of neat complexes. Furthermore, the Si and Al contents in M(II/IV)-Y and their imprisoned complexes were almost in the same ratio as in the parent zeolite. This indicated tiny changes in the zeolite structure due to lack of dealumination during metal ion exchange.

The textural properties of catalysts were quantified by means of BET technique (Table 2). The parent Na-Y possessed the biggest surface area and the biggest entire pore size. Contrarily on imprisoning the TMCs, surface vicinity and pore size significantly decreased in comparison to the parent Na-Y. This occurred due to the method of synthesis used for imprison of metal and ligand [38]. The decreased pore size of materials revealed that the encapsulation was occurring inside the cavity of zeolite-Y and not on the outside.

Scanning electron micrograph (SEM) technique was performed to check the crystallinity and purity of the zeolite. We took catalyst Co(HNIMMPP)(H_2O)]-Y and recorded micrographs beforehand and afterward Soxhlet extraction as presented in Fig. 5. This showed strongly defined rock crystal of zeolite imprisoned complexes

after Soxhlet extraction free from any shadow of the metal complex present on the exterior of zeolite [39].

The crystallites of the vacant zeolite possessed well defined orbicular grain like crystals. Given sample of encumbered zeolite also showed the orbicular rock crystals indicating that the zeolite crystallites were not affected by the imprisonment [40].

The X-ray powder diffraction shapes of [Fig. 6(a), (b)] were observed at 2θ (degree) values for studying crystallinity of Na-Y and their imprisoned transition metal complexes. XRD patterns of the zeolite-Y imprisoned complexes showed the diffraction lines of the neat zeolite that displayed no appreciable change in peak positions. This indicated that the crystallinity of the zeolitic framework stayed undamaged upon imprisonment of complex moiety [41]. Conversely, the comparative strengths of some of the diffraction lines underwent slight change because of imprisonment.

The data obtained by vibrational spectroscopy provided evidence on the reliability of the ligand (HNIMMPP), zeolite-Y imprisoned TMCs and the crystallinity of the host framework. The intensity of the bands of the imprisoned complex was feeble because of their low concentration in the matrix. The FT-IR spectroscopic statistics of the ligand (HNIMMPP) and their imprisoned TMCs were formulated and are presented in Table 3 and Fig. 7 respectively. The IR bands of imprisoned complexes were similar to those of the neat metal complexes. However, a significant change in some bands of the free ligand was observed. At ~1070 cm^{-1}a shrill band was obtained in all imprisoned complexes which were not observed in the equivalent neat complexes and in ligand Fig. 7. The zeolitic framework [TO_4 tetrahedral (T = Si or Al)] band dominated the spectra under 1200 cm^{-1} [42]. The bands detected at ~580, ~700, and ~1110 cm^{-1} were attributed to T−O (structure sensitive band) double ring, symmetric stretching and asymmetric stretching vibrations, respectively.

The bands of HNIMMPP and their imprisoned TMCs were evaluated for studying the coordinating mode of ligand in entrapped complexes. The spectroscopic studies of HNIMMPP showed sharp and strong band at 1603 cm^{-1} owing to the azomethine ($\nu_{(C=N)}$) group. This band indicated the hypsochromic impact in the

spectroscopic data of imprisoned complexes, leading to harmonization of nitrogen in the azomethine [43]. The side chain appeared at ~3190 and ~1690 cm^{-1} due to the occurrence of $\nu_{(N\text{-}H)}$ and $\nu_{(C=O)}$ groups of ligands (HNIMMPP) [44, 45] (Fig. 8). This showed that the ligands existence as keto-imine tautomer shown in Scheme 1. Additionally, we observed disappearance of phenolic -OH vibration of ligand (3380 cm^{-1}) from the entrapped complexes. The ligand responded in enol arrangement with prototrophy combined into proton transfer through oxygen atoms of the ligand, forming two bonds with the metal ion. All zeolite-Y imprisoned complexes displayed bands at 1135, 1020, 790, and 720 cm^{-1} owing to the host zeolite structure [46, 47]. No shift was observed upon introduction of metal ions and the inclusion of metal complexes. Introduction of metal ions and metal lead to no additional shift because the zeolite-Y framework remained an unaltered complex.

The ultra-violet spectroscopic data of ligand (HNIMMPP) and their VO(IV), Mn(II), Fe(II), Co(II), Ni(II) and Cu(II) based imprisoned complexes along with their respective neat complexes are tabularized in Table 4. The HNIMMPP ligand exhibited three bands at 223, 255, and 347 nm caused by intra-ligand charge transfer transitions $\pi \rightarrow \pi^*$. The bands of discrete neat complexes of VO(IV), Mn(II), Fe(II), Co(II), Ni(II) and Cu(II) were seen at 212 and 245 nm as similar to 223 and 255 bands in HNIMMPP ligand. However, $n \rightarrow \pi^*$ transition underwent hypsochromic shifts 368 nm in VO(IV), 386 nm in Mn(II), 396 nm in Fe(II), 390 nm in Co(II), 403 in Ni(II) and 409 nm in Cu(II) neat complexes ensuing from the chelation of the ligand with the transition metal as displayed in Fig. 9. These values were equivalent to the values for the imprisoned VO(IV), Mn(II), Fe(II), Co(II), Ni(II) and Cu(II) complexes observed at ~405 nm Fig. 10. Restriction of complexes within the nanopores of zeolite-Y was observed [48].

The *d-d* absorption spectroscopic data of VO(IV) complexes with square pyramidal geometry (C_{4v} symmetry) present three bands corresponding to the transitions $b_2 \rightarrow e$, $b_2 \rightarrow b_1$ and $b_2 \rightarrow a_1$ [49]. The distortion of the square pyramidal geometry was specified by splitting of the absorption bands [50]. The spectroscopic data of VO(IV) imprisoned complex showed two additional absorption bands at 570 and 699 nm due to $b_2 \rightarrow b_1$ and $b_2 \rightarrow e$ transitions, respectively [51]. In the electronic spectrum of entrapped complex Mn(II)-Y, the characteristic bands appeared at 316 and 242 nm due to $^6A_{1g} \rightarrow {}^4A_{1g}$, ^4E_g (v3) and metal to ligand charge transfer (MLCT)

transitions, respectively. This was due to distorting octahedral geometry covered to the metal ion. The electronic spectrum of Fe(II)-Y exhibited a band at 306 nm owing to MLCT transition. The non-appearance of *d-d* transitions in the spectroscopic data of imprisoned Fe(II) complex was caused by the lower concentration on the inner side the pores of zeolite-Y. Co(II)-Y showed bands at 421, 386, and 241 nm due to $^4T_{1g}(F) \rightarrow {}^4A_{2g}(F)$, $^4T_{1g}(F) \rightarrow {}^4T_{1g}(P)$, and MLCT transitions of an octahedral geometry around the metal ions. The absorption spectrum of Ni (II)-Y exhibited two bands at 406 and 237 nm due to $^3A_{2g} \rightarrow {}^3T_{1g}(P)$ (ν_3) and $^3A_{2g} \rightarrow {}^3T_{1g}(F)$ (ν_2) transitions respectively [52]. The electronic spectroscopic data of Cu(II)-Y consisting a band at 221 nm and a shoulder at 366 nm assigned to the $d_{xz,yz} \rightarrow d_{xy}$ and MLCT transitions for tetrahedrally distorted (D_{2h}) mononuclear copper(II) complexes respectively [53].

TGA curves are displayed in Fig. 11 and Fig. 12. For the analysis of all imprisoned complexes, the decomposition designs were discovered to be of similar type. At the initial stage, water molecule was removed followed by the decomposition of complex present into the zeolite cavities. Zeolite matrix was robust to decomposition from extreme temperature at 580-700 °C in the investigation. Only 20 to 30% mass loss was recorded till ~550 °C indicating the extraordinary thermal constancy of zeolite matrix and low loading of metal complex in the cavities.

3.2. Catalytic liquid-phase oxidative reaction of styrene

Catalytic liquid-phase oxidative reaction of styrene was performed by synthesized heterogeneous catalysts like zeolite-Y imprisoned TMCs using oxidant (TBHP). The outcome of these catalytic activities yielded benzaldehyde with the highest selectivity while styrene glycol, styrene oxide, and chalcone with less selectivity.

3.3. Optimism of catalysis

[VO(HNIMMPP)(H_2O)]-Y was used as a representative catalyst to optimize reaction conditions. The conditions included the impact of various solvents, the amount of catalyst, temperature, reaction time, oxidant and the mole ratio of reactant. The legible explanation for the oxidation of styrene was:

3.3.1. Impact of various solvents

The impact of a variety of solvents on the oxidative reaction of styrene was studied by keeping other reaction parameters fixed. Five different solvents viz., acetone, chloroform, acetonitrile, ethanol and carbon tetrachloride gave 81.10, 83.69, 93.35, 80.29 and 31.73% conversion to product respectively. As demonstrated in Fig. 13, the behaviour of styrene oxidation in various solvents was strikingly different. Acetonitrile provided the finest conversion results, followed by chloroform. These observations revealed the reduction in conversion (%) of styrene in acetone, chloroform, ethanol, and CCl_4 was due to the lower solubility of TBHP in the solvent as a result of which the reaction could not proceed fast. THBP and styrene were highly soluble in acetonitrile owing to its polar surface and high dielectric constant catalytic activity. It improved adsorptivity on the catalyst surface and augmented the effectiveness of the conversion. Polar solvents similar to acetonitrile simplified the establishment of active oxygen species and thus enhanced the catalytic activity [54].

3.3.2. Impact of quantity of catalyst

The quantity of catalytic agent had a noteworthy impact on the oxidative reaction of styrene. Dissimilar quantities of [VO(HNIMMPP)(H_2O)]-Y catalyst viz., 0.03, 0.05, 0.07 and 0.10 g were used by keeping other parameters static. The data shown in Fig. 14 indicated 52.18, 77.64, 93.35 and 93.13% conversion corresponding to 0.03, 0.05, 0.07 and 0.10 g catalyst respectively. Greater conversion percentage was observed with 0.07 g catalyst. When 0.10 g of catalytic agent was used, no further progress in the conversion was noticed. Therefore, 0.07 g quantity of catalytic agent was considered to be optimal.

3.3.3. Impact of temperature

The oxidative reaction of styrene was examined over the temperature range of 50 to 90 ˚C as presented in Fig. 15. The (%) of conversion styrene was increased from 60.41 to 93.35% for 10 h when the temperature was increased from 50 to 80 ˚C. Conversion of styrene decreased on heating at 90 ˚C. This was due to rapid decomposition of TBHP. By this we concluded that the optimum temperature was 80 ˚C for the oxidative reaction of styrene.

3.3.4. Impact of reaction period

As shown in Fig. 16, by cumulative reaction spell starting from 2-12 h, styrene conversion increased from 21.58 to 93.35%. Additional rise in reaction time didn't show any change in the conversion of styrene. Therefore, 10 h reaction time was considered as optimum.

3.3.5. Impact of mole ratio of reactant to oxidant

We used mole ratio of styrene to oxidant TBHP on oxidative reaction of styrene with four different mole ratios (1:1, 1:1.5, 1:2 and 1:2.5). Rest of the reaction parameters were taken at constant value (10 mL acetonitrile, 0.07 g VO(HNIMMPP)(H_2O)]-Y, 80 ˚C, 10 h). As displayed in Fig. 17, percentage conversion of styrene increases from 79.24 to 93.35% by increasing the mole ratio of styrene and TBHP from 1:1 to 1:2. This amount of oxidant was taken to be optimal as increase in the mole ratio to 1:2.5 lead to reduction in the styrene conversion to 90.19%. Concentration of TBHP was determined by iodometric method [56].

After optimization of reaction conditions, the oxidative reaction of styrene was performed by using Na-Y zeolite, metal exchanged zeolite-Y, neat complex and zeolite-Y imprisoned complexes as catalyst. In a usual reaction, TBHP as oxidants gives major products viz. benzaldehyde, styrene glycol, styrene oxide, and chalcone. Reaction conditions for the liquid-phase oxidative reaction of styrene were optimized as follows: styrene (30 mmol), 60 mmol of TBHP, catalyst (0.07 g), acetonitrile (10 mL) at the temperature point 80 ˚C for 10 h (Table 6) (Fig. 18).

As revealed in Table 6, negligible conversion occurs in the occurrence of Na-Y zeolite and metal exchanged zeolite-Y, suggesting that complexes were responsible of oxidative reaction of styrene. Therefore, zeolite-Y imprisoned complexes of all three series were tested over styrene oxidation under similar reaction conditions. The proportion transformation of styrene to benzaldehyde, styrene oxide, styrene glycol and chalcone are presented in Table 5 (Fig. 19). This clearly indicated that the styrene conversion varied from the catalyst to catalyst. The transformation of styrene by zeolite-Y imprisoned complexes increased in the order: [Mn(HNIMMPP)($H_2O)_3$]-Y<[Fe(HNIMMPP)($H_2O)_3$]-Y<[Co(HNIMMPP)(H_2O)]-Y<[Cu(HNIMMPP)(H_2O)]-Y<[Ni(HNIMMPP)(H_2O)]-Y<[VO(HNIMMPP)(H_2O)]-Y.

Amongst them, zeolite-Y imprisoned oxovanadium complexes exhibited exceptional performance by providing high catalytic transformation of styrene oxidation.

[VO(HNIMMPP)(H_2O)]-Y was run repeatedly three times to check the reusability of catalyst and the results are illustrated in Table 6 (Fig. 18). The used catalytic agent was recuperated and washed through an abundant quantity of condensed water and then by acetone after each catalytic run. Before reuse the washed [VO(HNIMMPP)(H2O)]-Y was dried at 100-120 ˚C for 22-24 h. After the primary cycle of the catalytic activity, it showed fall in the conversion with compared to fresh one. This fall in the activity was continuous with decline in the extent of vanadium content. This shortfall in the activity was due to low quantity of vanadium and excess quantity of ligand in the catalyst [VO(HNIMMPP)(H_2O)]-Y framework. The imprisoned complex reacted with reactant on the surface of catalyst with this ratio of vanadium and ligand in the reaction solution. Through the result of AAS analysis, this assumption of vanadium content in the reaction mixture confirmed. The content of vanadium in the catalyst remained unchanged with no significant catalytic activity drop after second cycle. The sensitive centers were afforded by the complex which was shielded through porous support of catalyst. This prevented decomposition and dimerization under reaction conditions and made it recoverable. This result showed that the catalytic agent was stable and ecological in the behavior with negligible change in the reactivity.

3.3.6. Catalytic reaction scheme

The catalytic reaction scheme [55] for the oxidative reaction of styrene by zeolite-Y imprisoned VO(IV) complexes is demonstrated in Scheme 2. Theoretically, this catalytic oxidation reaction of styrene may undergo through two possible paths. The catalytic agent reacted with TBHP to produce metal-oxo species (II). During the process, an active metal-oxo species (II) attacked double bond. The >C=C< double bond of styrene molecule furnished an intermediary species (III) by oxidative addition of metal-oxo species •OOV^{5+}L/NaY. This intermediary species furnished cyclic styrene oxide (IV) and regenerated OV^{4+}L/NaY. On reaction with H^+/H_2O styrene oxide (IV) furnished styrene glycol (V).

Styrene oxide reacted with metal-oxo species (II) to produce benzaldehyde (VII) through intermediate (VI). In another pathway, species (II) attacked styrene to produce species (VIII) which formed acetophenone through intermediate (IX). Hydroxylation reaction between benzaldehyde and acetophenone yielded chalcone (XI) as the final product with the removal of water.

4. Conclusion

Our study deals with the creation of Schiff base ligand, its transition metal complexes, metal ion exchanged zeolite-Y and zeolite-Y imprisoned TMCs of HNIMMPP. Characterization of that neat and imprisoned zeolite-Y complexes and catalytic oxidative reaction of styrene by the zeolite-Y imprisoned M(II/IV) TMCs were done over the liquid-phase using TBHP as an oxidant. During these catalytic studies of styrene, we found that all these imprisoned complexes were more efficient catalysts then their uncaged complexes and zeolite-Y in the liquid-phase catalytic oxidation. Styrene gave benzaldehyde, styrene oxide, styrene glycol and chalcone as major products at a time of the reaction. A study was carried out to get optimum situations by altering the amount of catalysts, solvent, amount of catalyst, temperature, the mole ratio of oxidant and time. Studies of catalytic oxidation showed more selectivity towards benzaldehyde from styrene. The result of catalytic oxidative reaction of styrene, among series of imprisoned catalysts [VO(HNIMMPP)(H_2O)]-Y showed the highest percentage of conversion i.e. 93.35%. The recyclability revealed that these imprisoned complexes truly performed as heterogeneous catalysts.

Acknowledgement

The writers are grateful to the UGC, New Delhi and Department of Science and Technology, New Delhi for economically backing under the NON-SAP and DST-FIST programs, respectively. Mr. Krunalsinh A Jadeja is thankful to UGC, New Delhi for UGC-MRP Project Fellowship. Mr. Bonny Y Patel is thankful to CSIR, New Delhi for CSIR EMR-II Senior Research Fellowship.

References

[1] J.L.F. Monteiro, C.O. Veloso, Top. Catal., 27 (2004) 169-180.

[2] P. Oliveira, M.L. Rojas-Cervantes, A.M. Ramos, I.M. Fonseca, A.M.B. do Rego, J. Vital, Catal. Today, 118 (2006) 307-314.

[3] W.E. Erman. Chemistry of the Monoterpenes. An Encyclopedic Handbook, Marcel Dekker, p. 12, New York, (1985).

[4] H. Mimoun, CHIMIA International Journal for Chemistry, 50 (1996) 620-625.

[5] M. Salavati-Niasari, P. Salemi, F. Davar, J. Mol. Catal. A: Chem., 238 (2005) 215-222.

[6] S.G. Baca, M.T. Reetz, R. Goddard, I.G. Filippova, Y.A. Simonov, M. Gdaniec, N. Gerbeleu, Polyhedron, 25 (2006) 1215-1222.

[7] A. Stamatis, C. Vartzouma, M. Louloudi, Catal. Commun., 12 (2011) 475-479.

[8] C. Vartzouma, E. Evaggellou, Y. Sanakis, N. Hadjiliadis, M. Louloudi, J. Mol. Catal. A: Chem., 263 (2007) 77-85.

[9] F. Hoelderich Wolfgang, F. Kollmer, in: Pure Appl. Chem., 2000, pp. 1273.

[10] M.H. Valkenberg, W.F. Hölderich, Catalysis Reviews, 44 (2002) 321-374.

[11] J. Čejka, G. Centi, J. Perez-Pariente, W.J. Roth, Catal. Today, 179 (2012) 2-15.

[12] C. Jiménez-Sanchidrián, J.R. Ruiz, Tetrahedron, 64 (2008) 2011-2026.

[13] N.E. Leadbeater, M. Marco, Chem. Rev., 102 (2002) 3217-3274.

[14] C.A. McNamara, M.J. Dixon, M. Bradley, Chem. Rev., 102 (2002) 3275-3300.

[15] D.C. Sherrington, A.P. Kybett, Supported catalysts and their applications, Royal Society of Chemistry, 2001.

[16] S.V. Ley, I.R. Baxendale, R.N. Bream, P.S. Jackson, A.G. Leach, D.A. Longbottom, M. Nesi, J.S. Scott, R.I. Storer, S.J. Taylor, J. Chem. Soc., Perkin Trans. 1, (2000) 3815-4195.

[17] D.C. Sherrington, Catal. Today, 57 (2000) 87-104.

[18] S. Kulkarni, M. Alurkar, A. Kumar, Applied Catalysis A: General, 142 (1996) 243-254.

[19] L. Daraiswany, M. Sharma, Heterogeneous Reaction: Analysis, example and reactor design, John Wiley & Sons, New York, 1984.

[20] P. Hodge, D.C. Sherrington, Polymer-supported reactions in organic synthesis, J. Wiley, 1980.

[21] F.G. Helfferich, Ion exchange chromatography, McGraw-Hill, 1962.

[22] Y. Goldberg. Phase Transfer Catalysis, Gordon and Breach, Switzerland, 1992.

[23] Y. de Miguel, Chem. Soc., Perkin Trans, 1 (2000) 4213-4221.

[24] D. Rechavi, M. Lemaire, Chem. Rev., 102 (2002) 3467-3494.

[25] D.E. De Vos, M. Dams, B.F. Sels, P.A. Jacobs, Chem. Rev., 102 (2002) 3615-3640.

[26] H.S. Abbo, S.J.J. Titinchi, Top. Catal., 53 (2010) 254-264.

[27] D. Srinivas, S. Sivasanker, Catalysis Surveys from Asia, 7 (2003) 121-132.

[28] P.-P. Knops-Gerrits, D. De Vos, F. Thibault-Starzyk, P.A. Jacobs, Nature, 369 (1994) 543-546.

[29] K. Srinivasan, P. Michaud, J.K. Kochi, J. Am. Chem. Soc., 108 (1986) 2309-2320.

[30] R. Irie, Y. Ito, T. Katsuki, Synlett, 1991 (1991) 265-266.

[31] V. Hulea, E. Dumitriu, Applied Catalysis A: General, 277 (2004) 99-106.

[32] S.B. Kumar, S.P. Mirajkar, G.C.G. Pais, P. Kumar, R. Kumar, J. Catal., 156 (1995) 163-166.

[33] M.R. Maurya, A. Kumar, M. Ebel, D. Rehder, Inorg. Chem., 45 (2006) 5924-5937.

[34] M.R. Maurya, A.K. Chandrakar, S. Chand, J. Mol. Catal. A: Chem., 278 (2007) 12-21.

[35] M.R. Maurya, A.K. Chandrakar, S. Chand, J. Mol. Catal. A: Chem., 263 (2007) 227-237.

[36] C. Saux, L.B. Pierella, Applied Catalysis A: General, 400 (2011) 117-121.

[37] K.R. Surati, B.T. Thaker, J. Coord. Chem., 59 (2006) 1191-1202.

[38] J. Haber, K. Pamin, J. Połtowicz, J. Mol. Catal. A: Chem., 224 (2004) 153-159.

[39] V.K. Bansal, P.P. Thankachan, R. Prasad, Applied Catalysis A: General, 381 (2010) 8-17.

[40] A. Nezamzadeh-Ejhieh, E. Shahriari, Journal of Industrial and Engineering Chemistry, 20 (2014) 2719-2726.

[41] M. Salavati-Niasari, F. Davar, Synthesis and Reactivity in Inorganic, Metal-Organic, and Nano-Metal Chemistry, 40 (2010) 345-354.

[42] V. Arun, N. Sridevi, P.P. Robinson, S. Manju, K.K.M. Yusuff, J. Mol. Catal. A: Chem., 304 (2009) 191-198.

[43] C.K. Modi, D.H. Jani, H.S. Patel, H.M. Pandya, Spectrochimica Acta Part A: Molecular and Biomolecular Spectroscopy, 75 (2010) 1321-1328.

[44] H. Zhao, Z. Zhang, Z. Zhao, R. Yu, Y. Wan, M. Lan, Adv Mat Lett, 2 (2011) 172.

[45] C. K. Modi, P.M. Trivedi, Advanced Materials Letters, 3 (2012) 149-153.

[46] C.K. Modi, D.H. Jani, Appl. Organomet. Chem., 25 (2011) 429-436.

[47] M.J. Alcón, A. Corma, M. Iglesias, F. Sánchez, J. Organomet. Chem., 655 (2002) 134-145.

[48] B. Fan, W. Fan, R. Li, J. Mol. Catal. A: Chem., 201 (2003) 137-144.

[49] C.J. Ballhausen, H.B. Gray, Inorg. Chem., 1 (1962) 111-122.

[50] E. Garribba, G. Micera, A. Panzanelli, D. Sanna, Inorg. Chem., 42 (2003) 3981-3987.

[51] E.G. Ferrer, M.V. Salinas, M.J. Correa, F. Vrdoljak, P.A. Williams, Zeitschrift für Naturforschung B, 60 (2005) 305-311.

[52] N.M. El-Metwaly, Transition Met. Chem., 32 (2007) 88-94.

[53] A.H. Maki, B. McGarvey, The Journal of Chemical Physics, 29 (1958) 35-38.

[54] M. Salavati-Niasari, Inorg. Chim. Acta, 362 (2009) 2159-2166.

[55] C.K. Modi, J.A. Chudasama, H.D. Nakum, D.K. Parmar, A.L. Patel, J. Mol. Catal. A: Chem., 395 (2014) 151-161.

[56] J. G. Hill, B. E. Rossiter and K. B. Sharpless, J. Org. Chem., 1983, 48, 3607

Figure Captions

Fig. 1 Synthesis of PMFP.

Fig. 2 Synthesis of Schiff base ligand HNIMMPP.

Fig. 3 Synthesis of Neat Transition metal complexes.

Fig. 4 Synthesis green cycle of zeolite-Y imprisoned transition metal complex.

Fig. 5 SEM pictures of [Co(HNIMMPP)H_2O]-Y with (A) Before and (B) After Soxhlet extraction.

Fig. 6 XRD shapes of (a) Na-Y and metal ion exchanged zeolite-Y (b) Na-Y and zeolite-Y imprisoned transition metal complexes.

Fig. 7 FT-IR spectroscopic data of Na-Y and their imprisoned transition complexes.

Fig. 8 FT-IR spectroscopic data of ligand and their uncaged complexes.

Fig. 9 Electronic spectroscopic data of Schiff base ligand and transition metal complexes.

Fig. 10 Electronic spectroscopic data of zeolite-Y imprisoned transition metal complexes.

Fig. 11 TGA curves of HNIMMPP and their uncaged complex.

Fig. 12 TGA curves of zeolite-Y imprisoned complexes.

Fig. 13 Impact of various solvents on the oxidative reaction of styrene.

Fig. 14 Impact of quantities of catalysts on the oxidative reaction of styrene.

Fig. 15 Impact of temperature on the oxidative reaction of styrene.

Fig. 16 Impact of reaction time on the oxidative reaction of styrene.

Fig. 17 Impact of Mole ratio of styrene to TBHP on the oxidative reaction of styrene.

Fig. 18 Oxidative reaction of styrene with TBHP as oxidant catalyzed by Na-Y, VO-Y, [VO(HNIMMPP)(H_2O)], [VO(HNIMMPP)(H_2O)]-Y.

Fig. 19 Oxidative reaction of styrene with TBHP as oxidant catalyzed by [M(HNIMMPP)(xH_2O)]-Y.

Scheme 1 keto-imine tautomer of Schiff base ligand.

Scheme 2 Plausible reaction mechanism of the catalytic oxidative reaction of styrene.

List of Figures

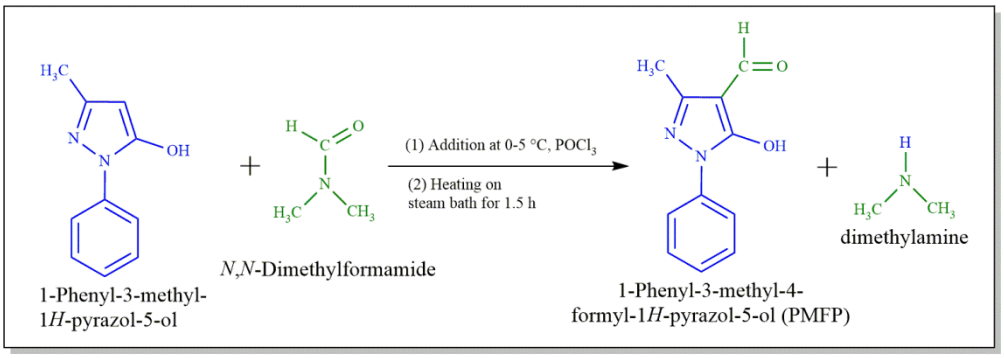

Fig. 1

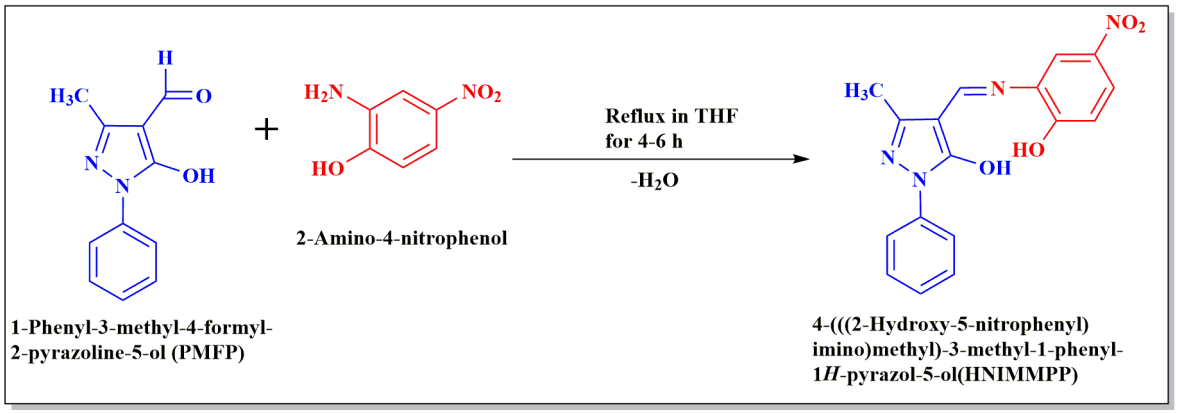

Fig. 2

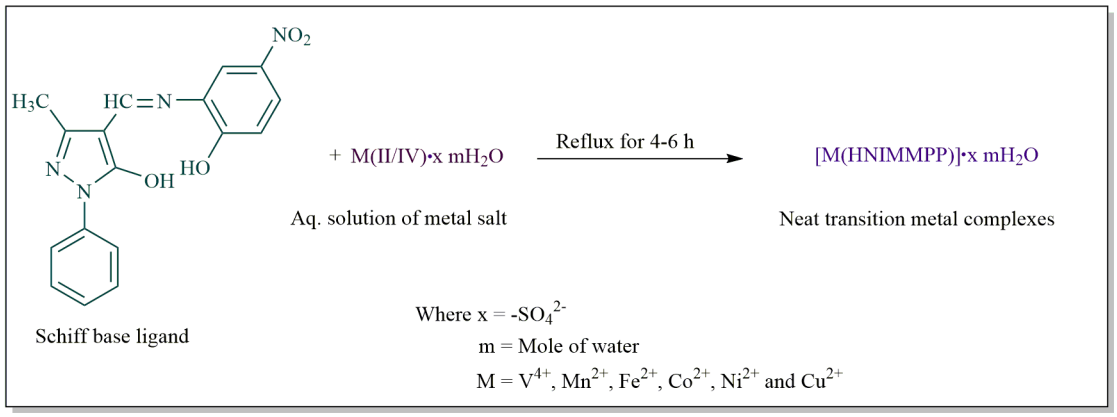

Fig. 3

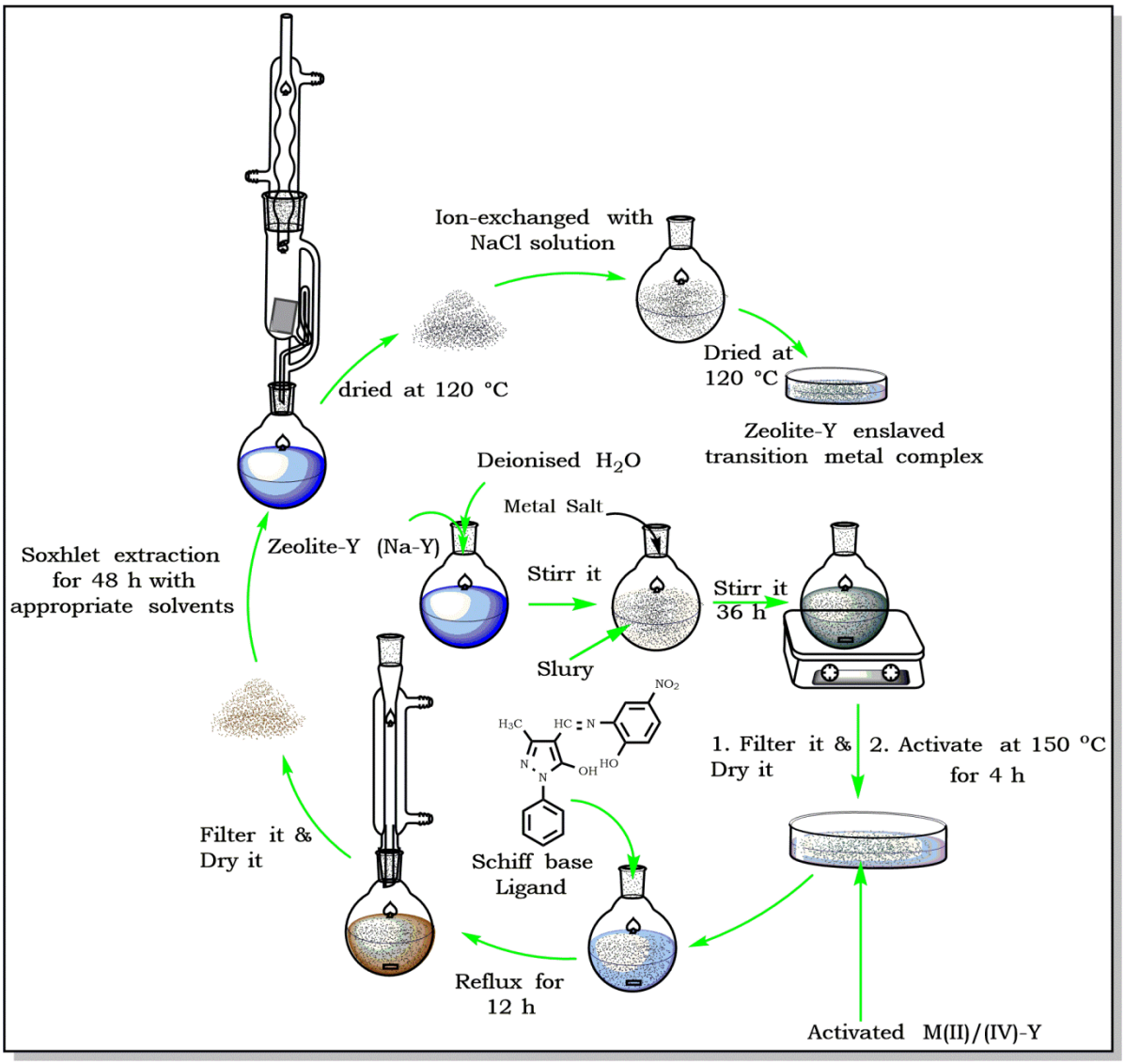

Fig. 4

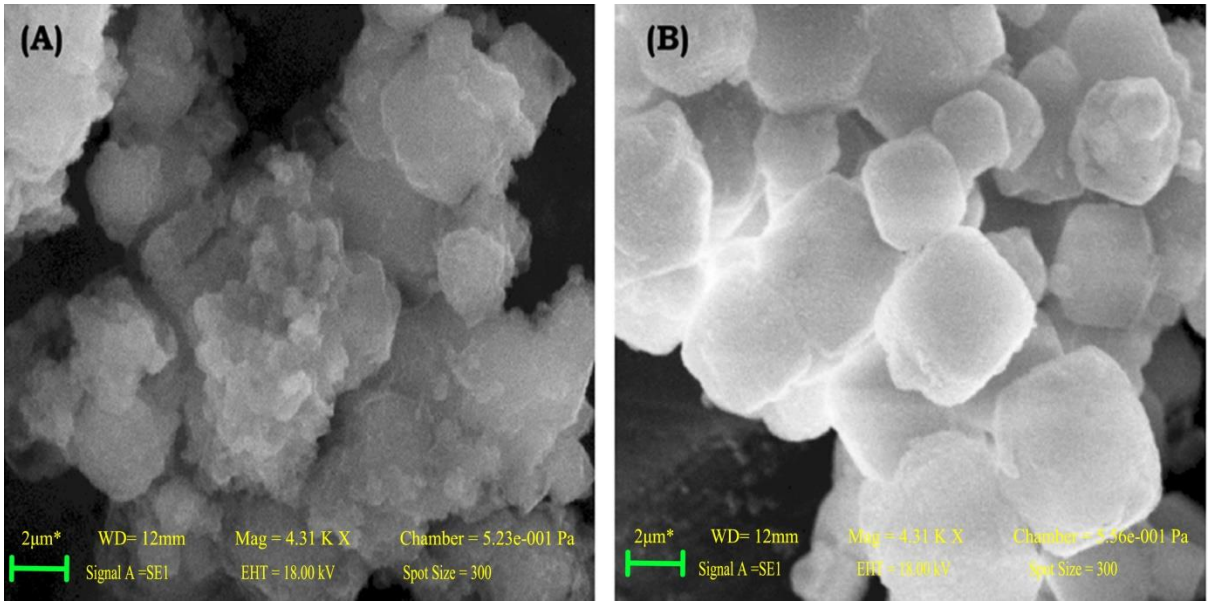

Fig. 5

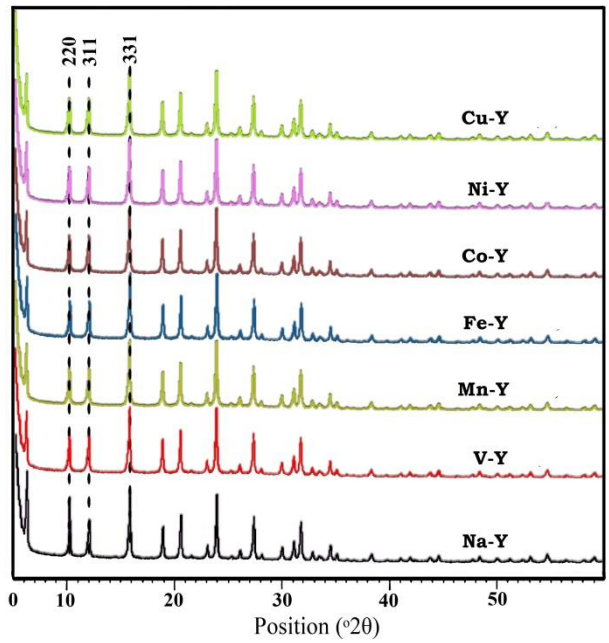

(a)

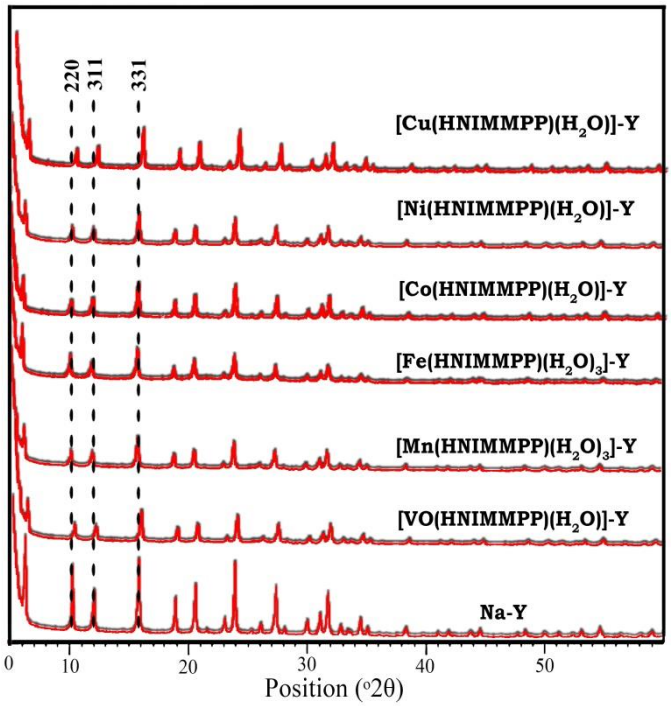

(b)

Fig. 6

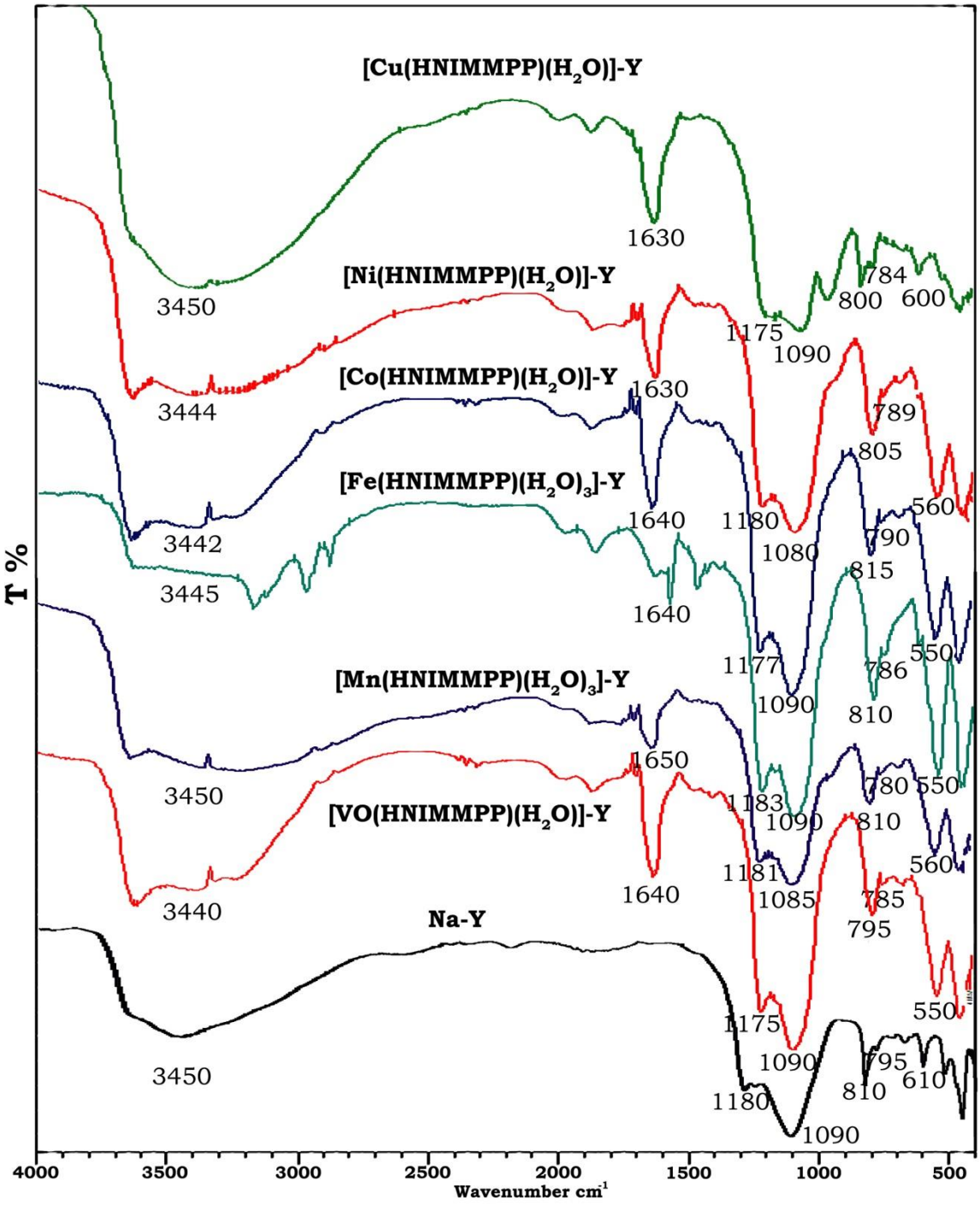

Fig. 7

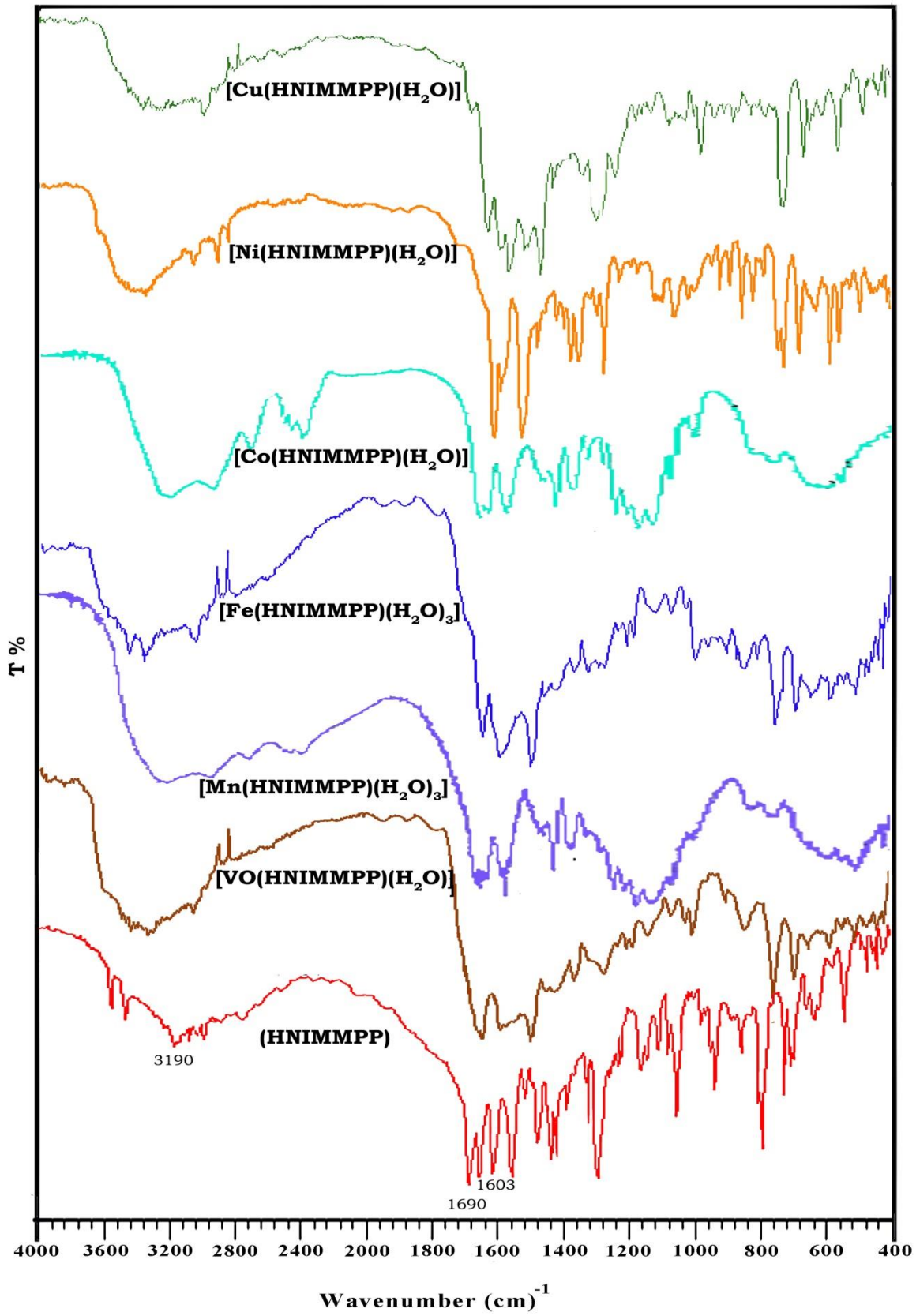

Fig. 8

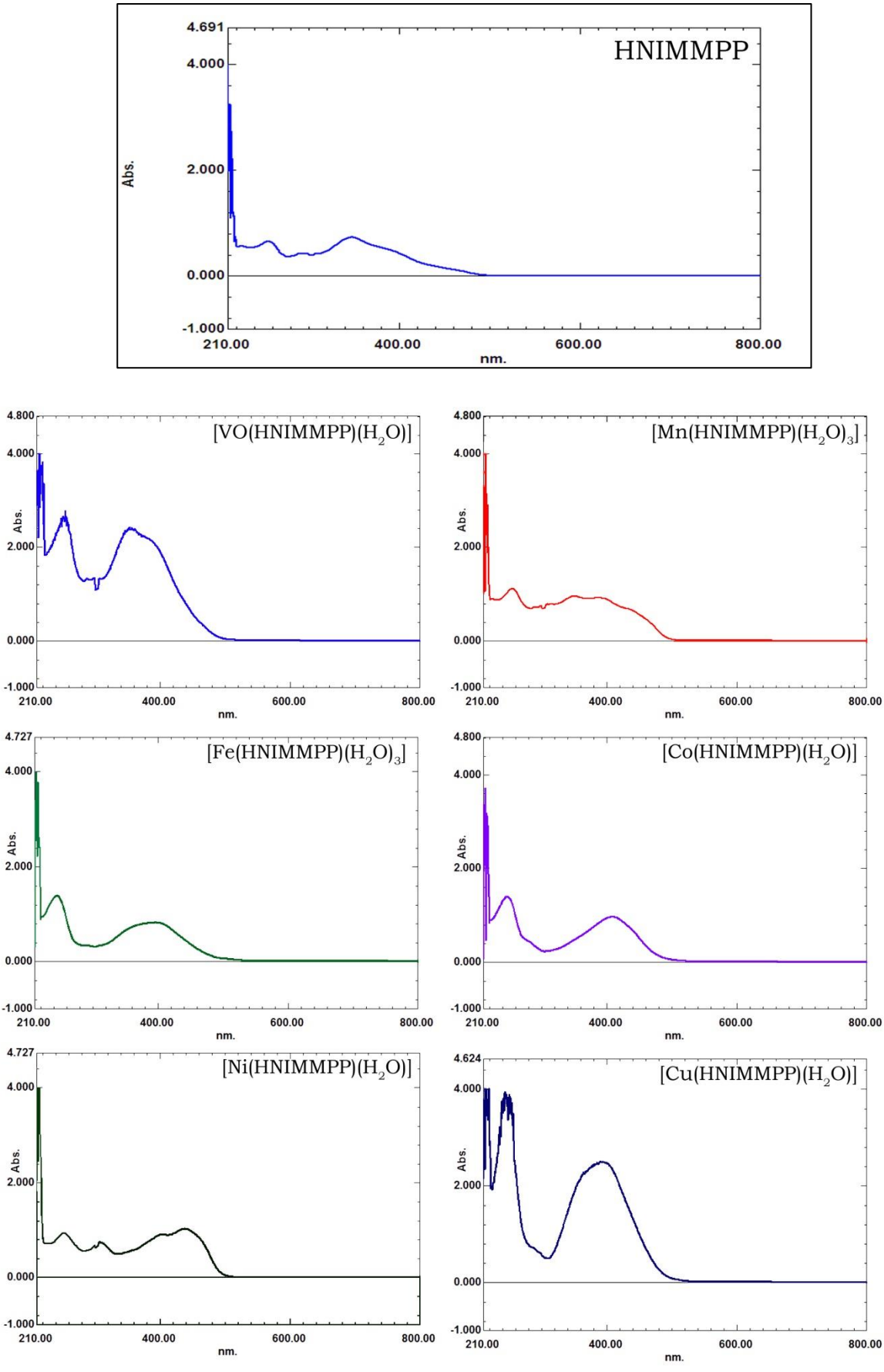

Fig. 9

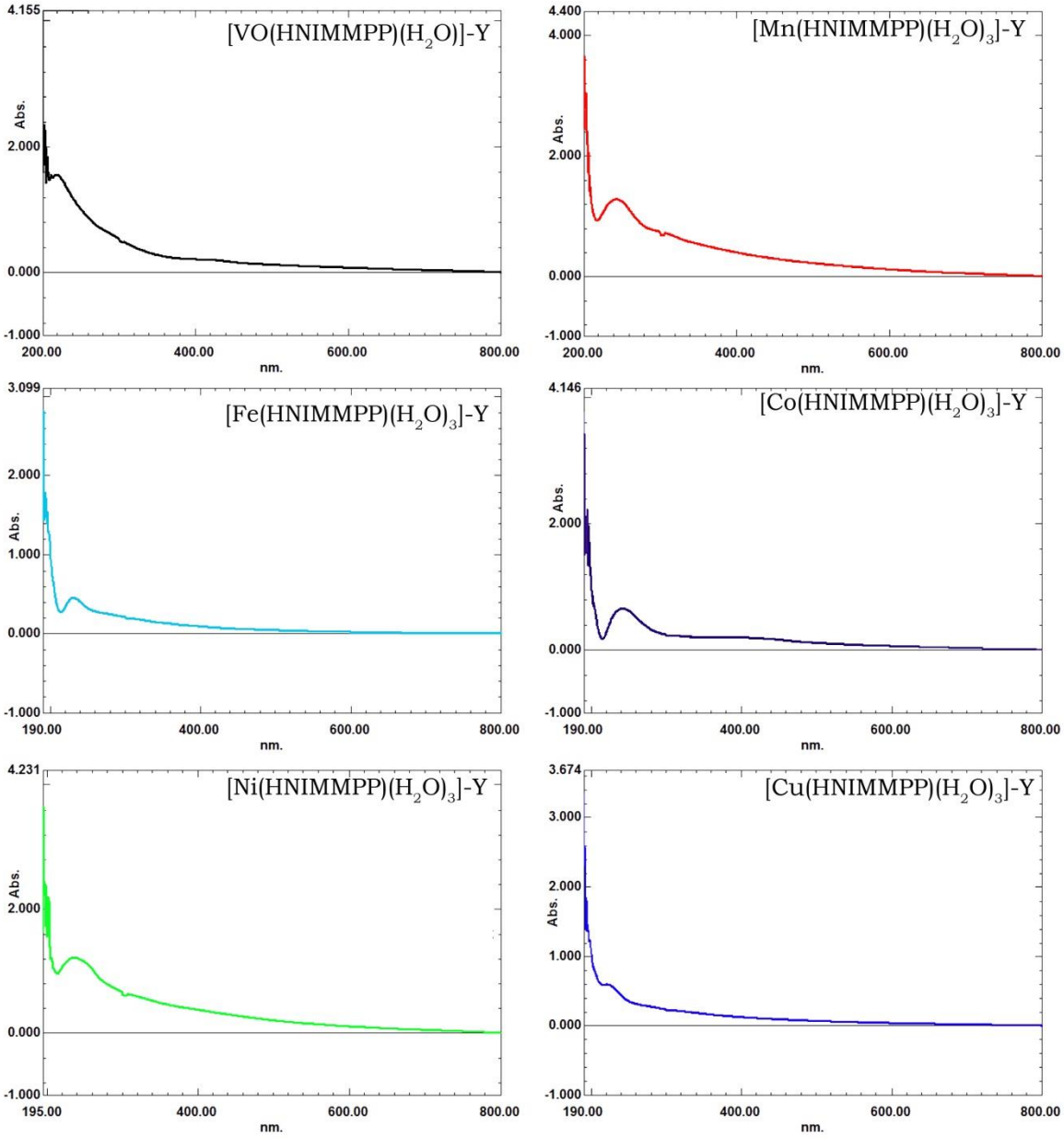

Fig. 10

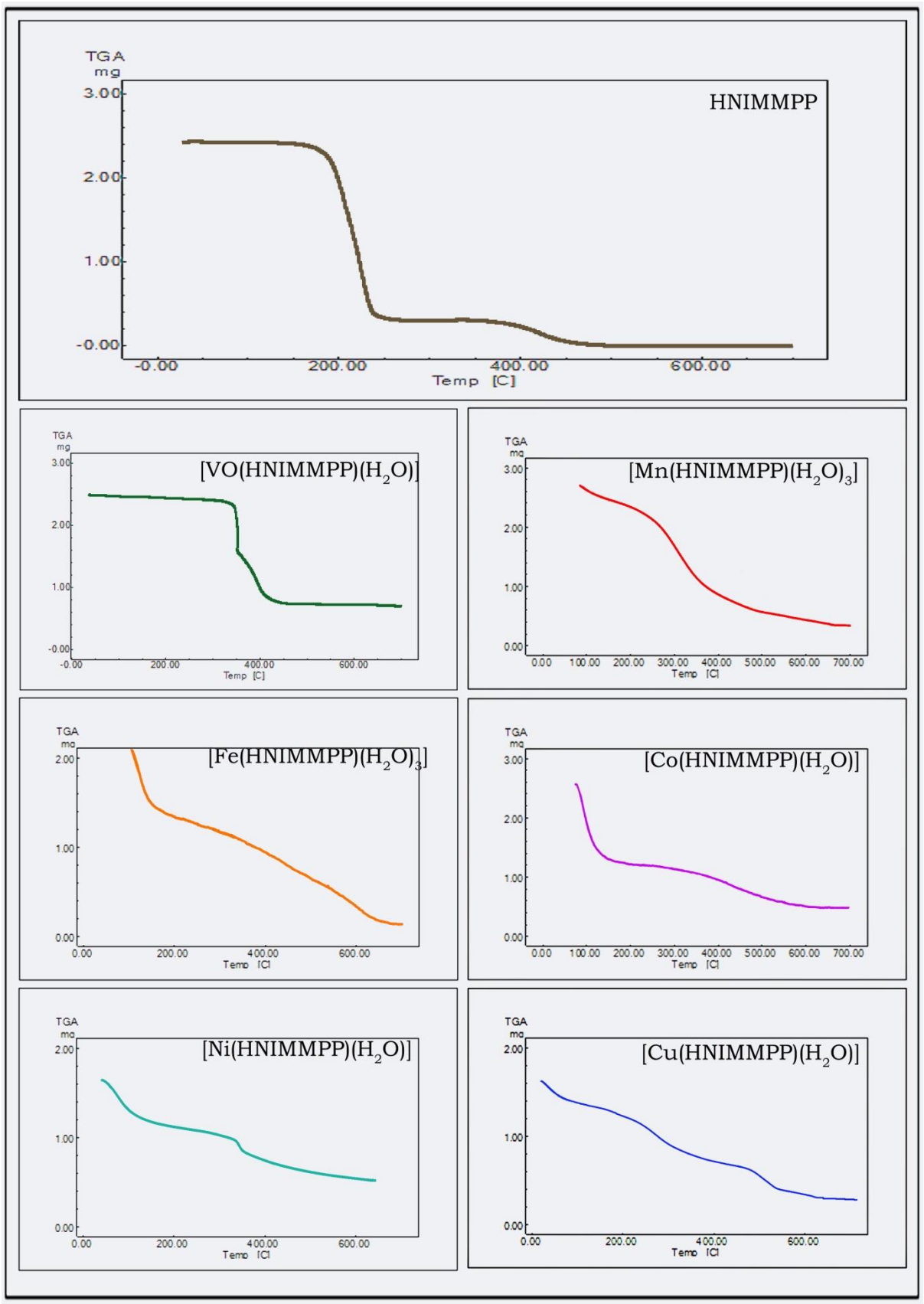

Fig. 11

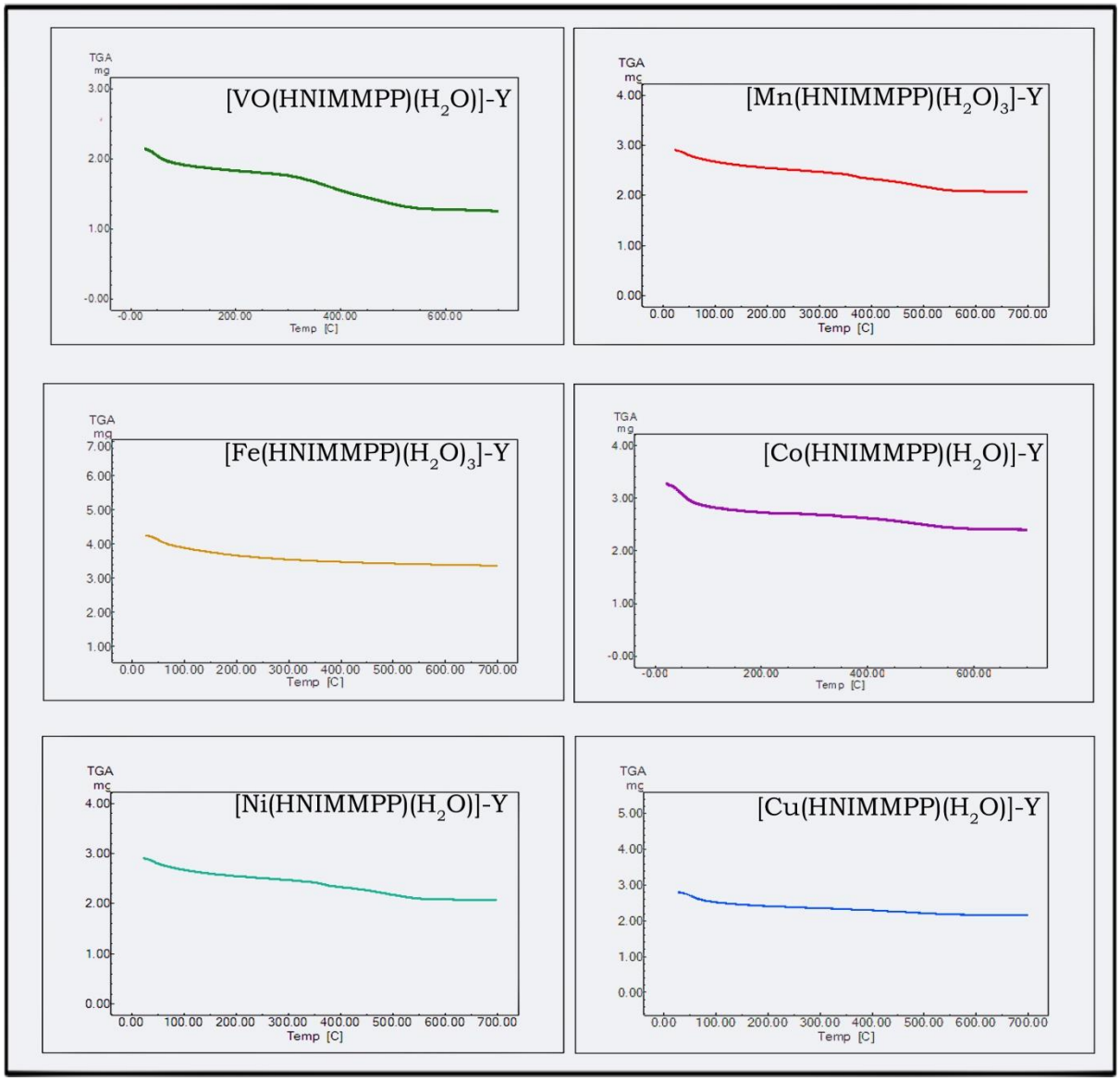

Fig. 12

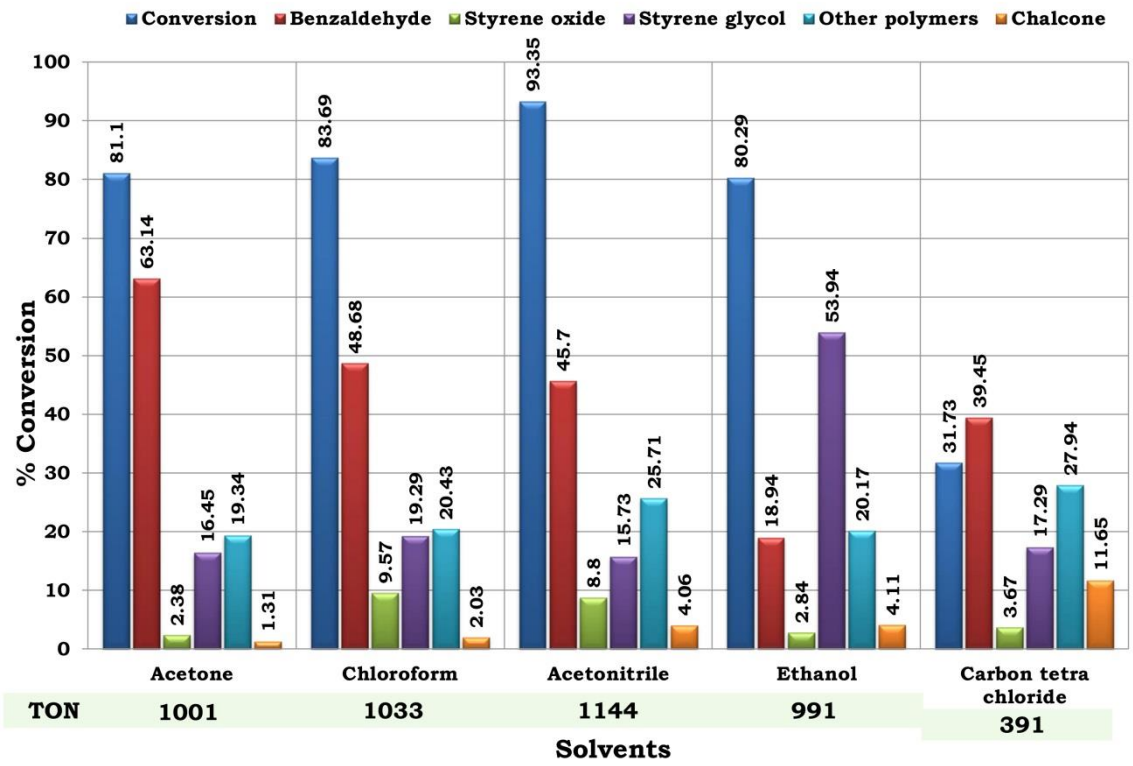

Fig. 13

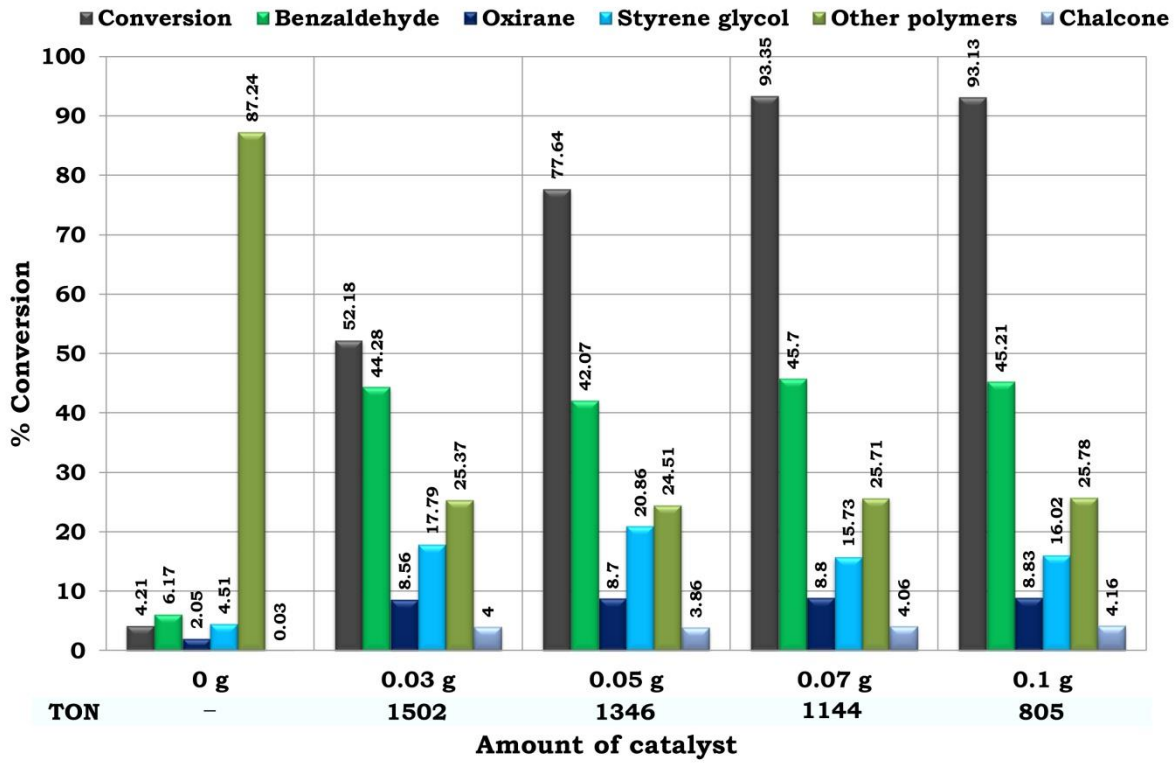

Fig. 14

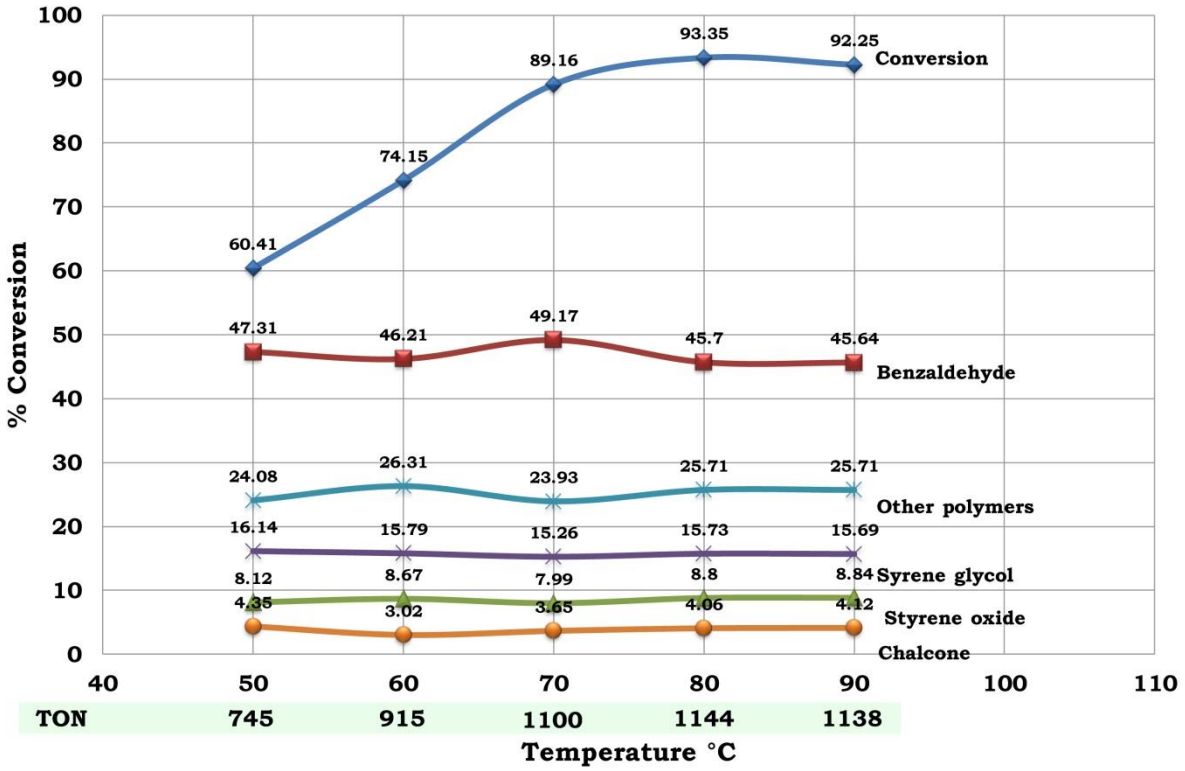

Fig. 15

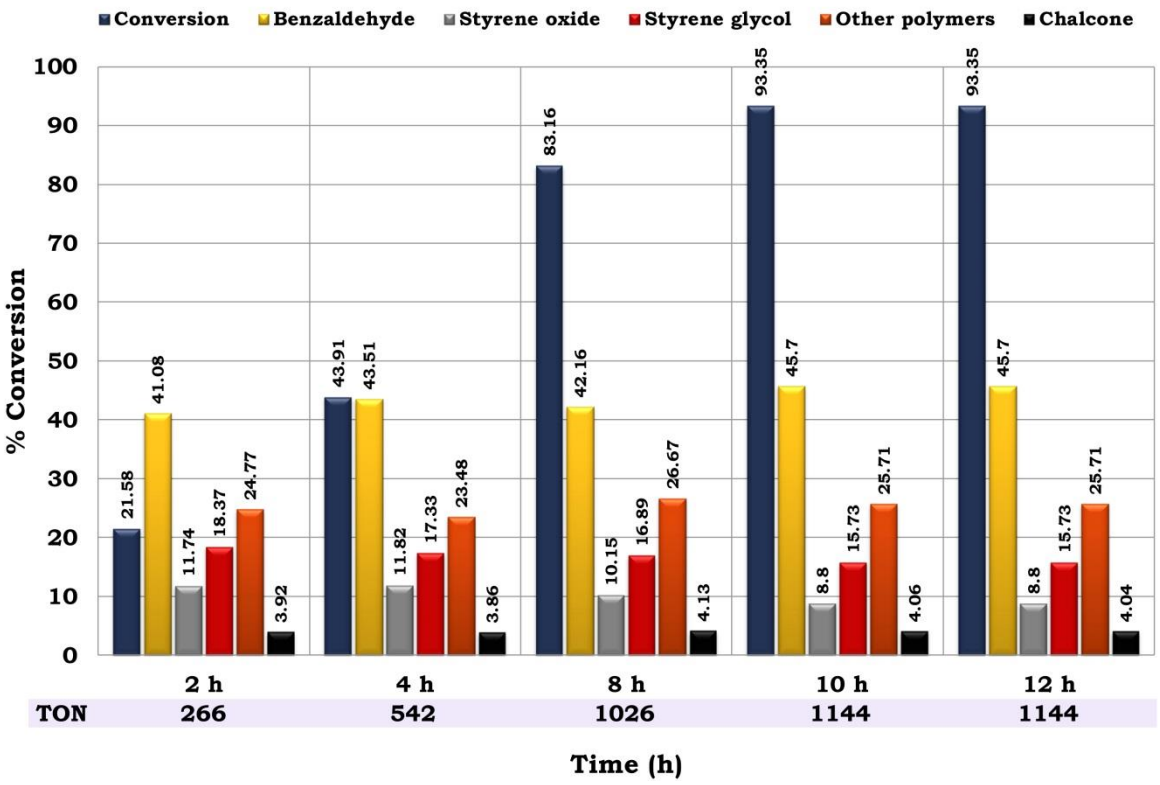

Fig. 16

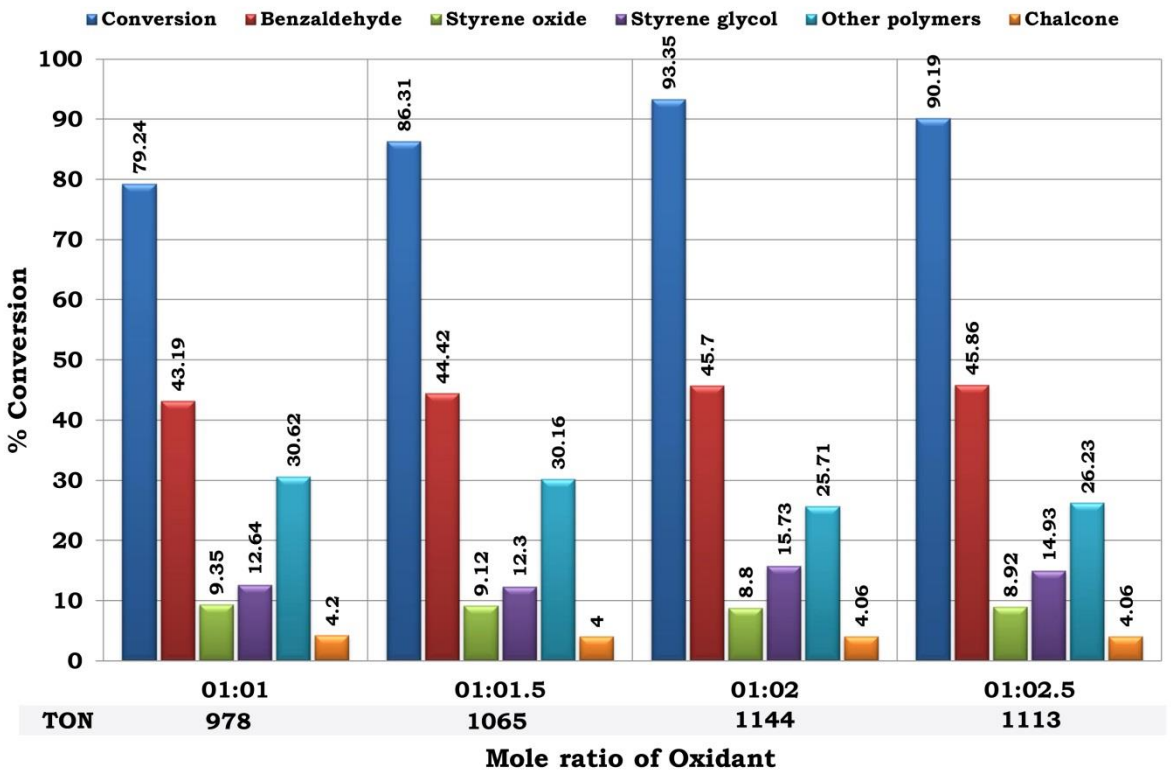

Fig. 17

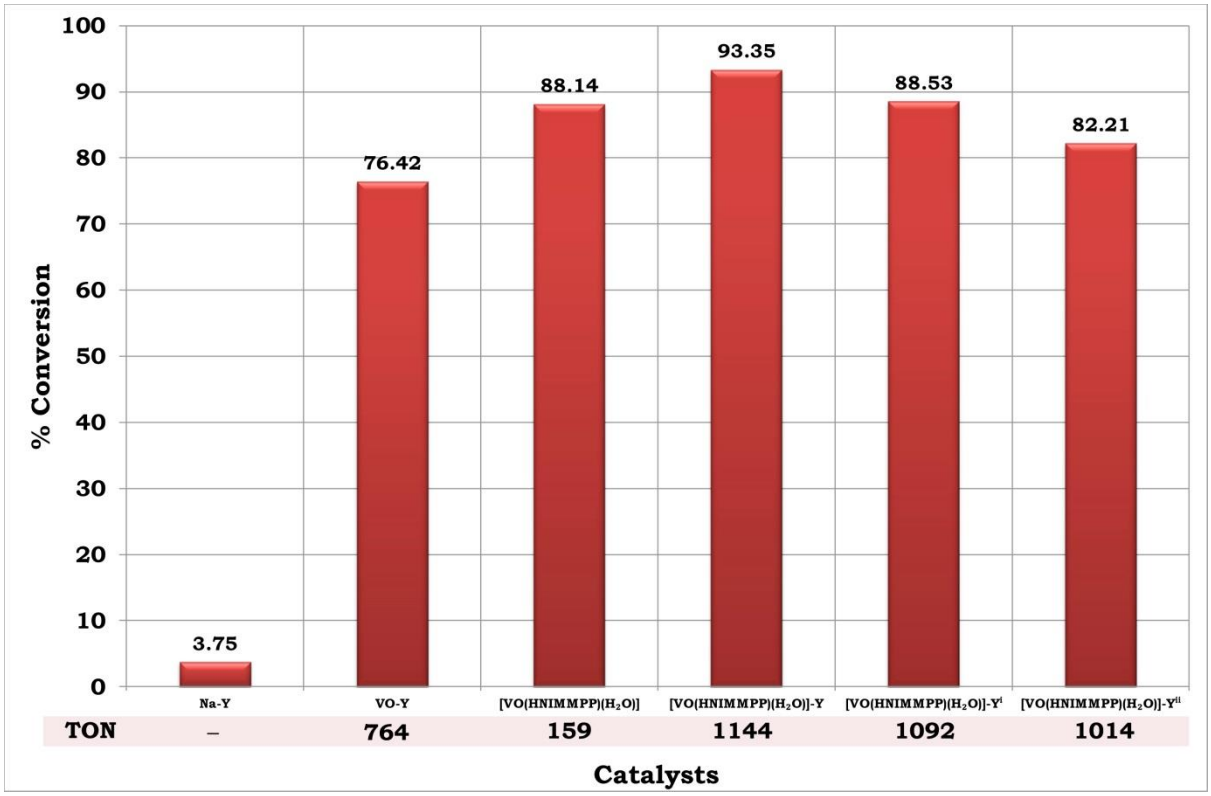

Fig. 18

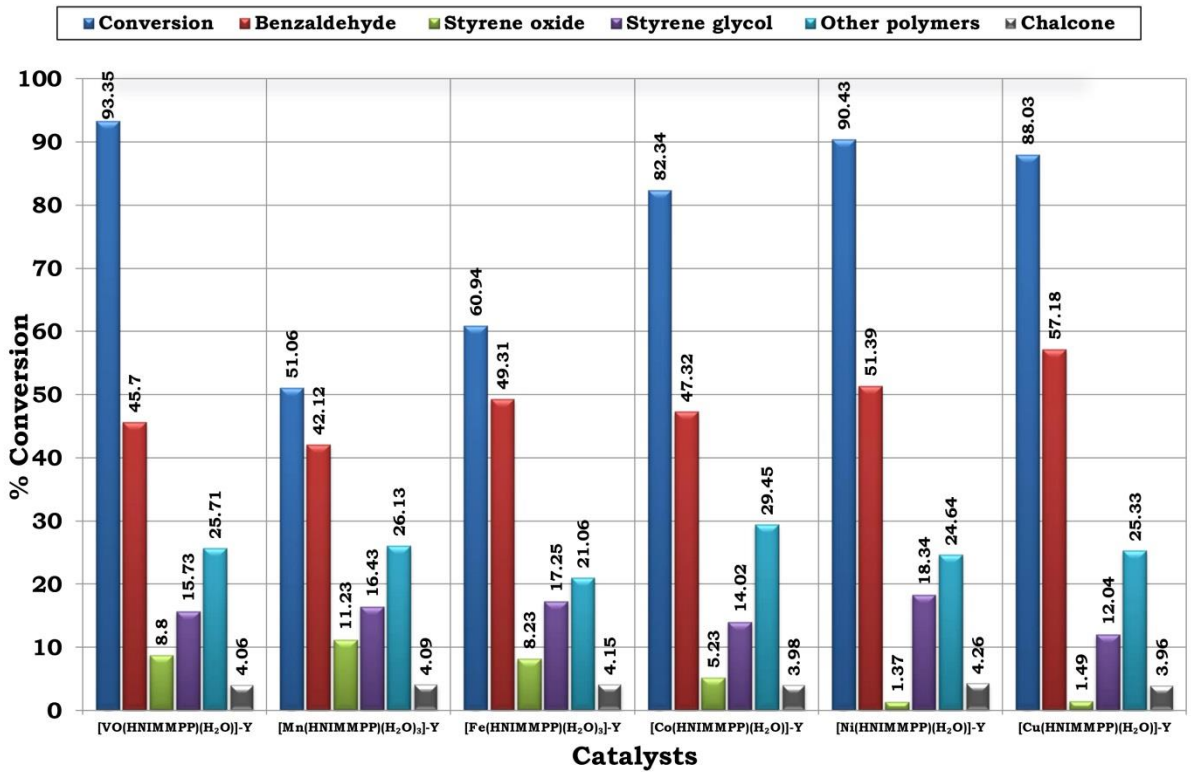

Fig. 19

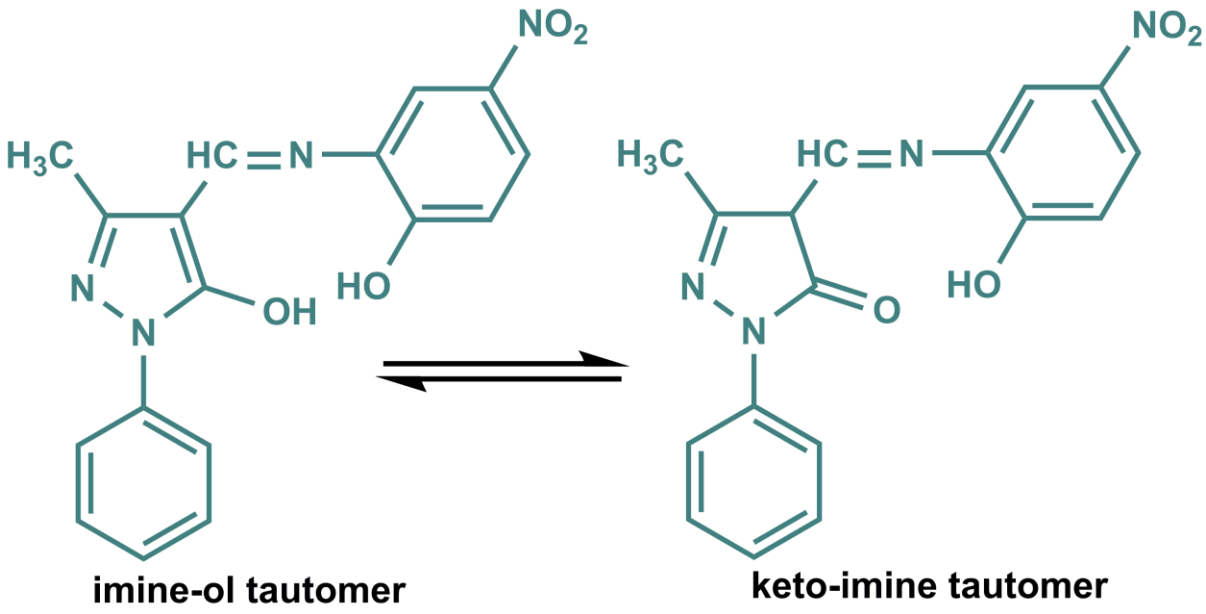

Scheme 1

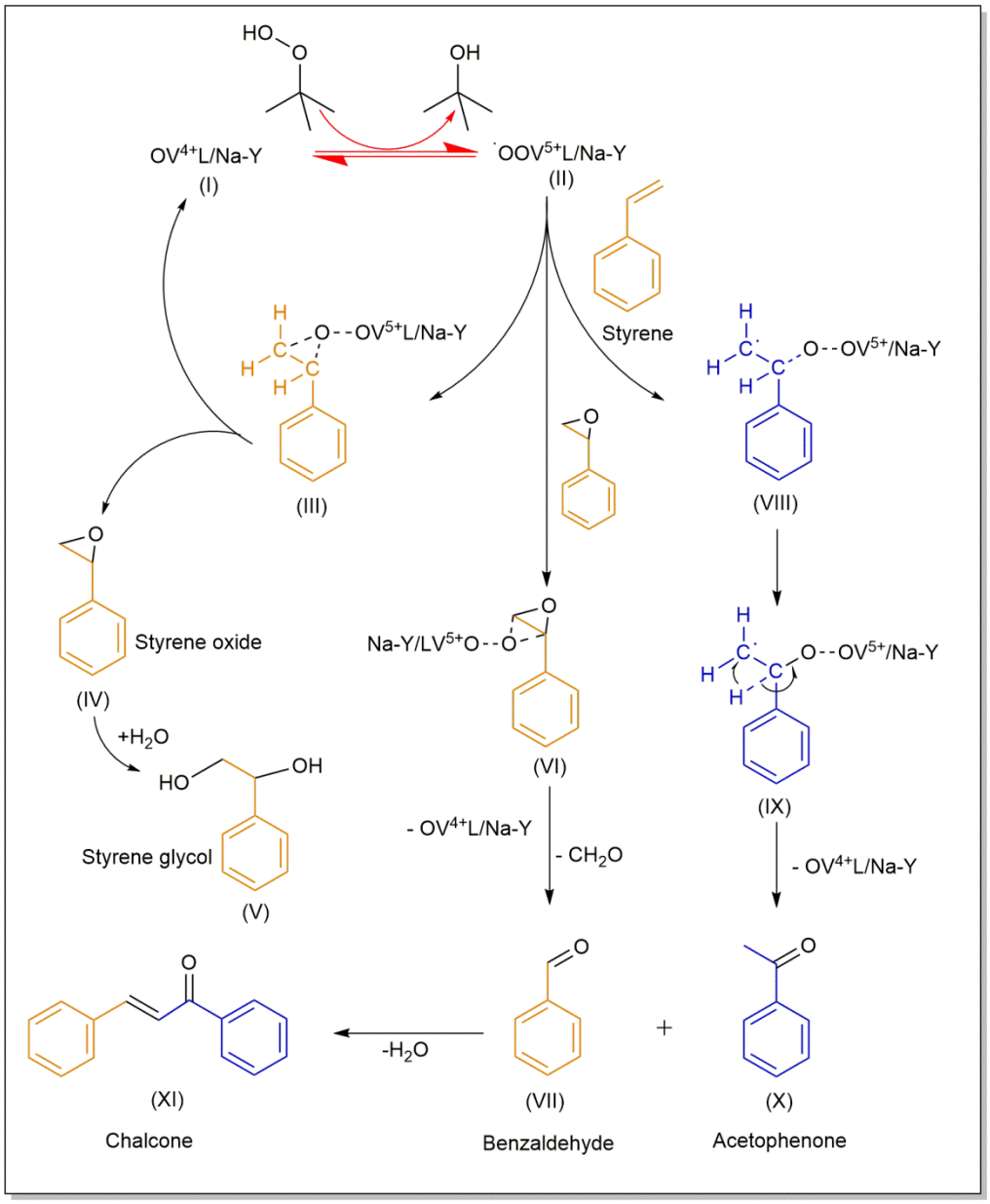

Scheme 2

List of Tables

Table 1 Analytical and physical data of materials.

Compound	Elemental analysis Found (Calculated)				Ratio (%)			
	C (%)	H (%)	N (%)	M(%)	C/N	Si (%)	Al (%)	Si/Al
Na-Y	-	-	-	-	-	17.16	6.60	2.50
[VO(HNIMMPP)(H_2O)]	48.21 (48.47)	3.09 (3.35)	12.84 (13.30)	12.09 (12.09)	3.75 (3.64)	-	-	-
[Mn(HNIMMPP)(H_2O)$_3$]	45.80 (45.85)	3.94 (4.07)	12.52 (12.58)	12.04 (12.34)	3.65 (3.64)	-	-	-
[Fe(HNIMMPP)(H_2O)$_3$]	45.72 (45.76)	3.94 (4.07)	12.56 (12.56)	12.44 (12.52)	3.65 (3.65)	-	-	-
[Co(HNIMMPP)(H_2O)]	49.40 (49.41)	3.36 (3.41)	13.52 (13.56)	14.33 (14.26)	3.65 (3.64)	-	-	-
[Ni(HNIMMPP)(H_2O)]	41.22 (41.23)	2.75 (2.85)	14.11 (14.14)	25.59 (25.63)	2.92 (2.92)	-	-	-
[Cu(HNIMMPP)(H_2O)]	48.88 (48.86)	3.32 (3.38)	13.44 (13.41)	15.22 (15.21)	3.64 (3.64)	-	-	-
[VO(HNIMMPP)(H_2O)]-Y	5.92	0.78	0.45	1.78	3.32	16.56	6.65	2.49
[Mn(HNIMMPP)(H_2O)$_3$]-Y	4.54	0.98	0.33	1.50	3.02	16.96	6.82	2.49
[Fe(HNIMMPP)(H_2O)$_3$]-Y	4.50	0.96	0.34	1.65	2.72	16.42	6.60	2.49
[Co(HNIMMPP)(H_2O)]-Y	6.16	0.84	0.48	1.96	3.14	16.45	6.60	2.50
[Ni(HNIMMPP)(H_2O)]-Y	4.08	0.63	0.55	2.36	1.72	16.52	6.63	2.50
[Cu(HNIMMPP)(H_2O)]-Y	6.07	0.81	0.46	2.06	2.94	16.45	6.58	2.50

Table 2 Specific surface area measurement data of Na-Y, M-Y and their imprisoned complexes.

Compound	Specific Surface area (m^2/g)	specific pore volume (cm^2/g)	Compound	Specific Surface area (m^2/g)	specific pore volume (cm^2/g)
Na-Y	630	0.210	**[VO(HNIMMPP)(H_2O)]-Y**	472	0.142
V-Y	539	0.1.66	**[Mn(HNIMMPP)(H_2O)$_3$]-Y**	527	0.156
Mn-Y	607	0.205	**[Fe(HNIMMPP)(H_2O)$_3$]-Y**	356	0.111
Fe-Y	571	0.190	**[Co(HNIMMPP)(H_2O)]-Y**	404	0.120
Co-Y	574	0.161	**[Ni(HNIMMPP)(H_2O)]-Y**	429	0.141
Ni-Y	551	0.172	**[Cu(HNIMMPP)(H_2O)$_3$]-Y**	321	0.094
Cu-Y	587	0.184			

Table 3 FTIR spectral studies of Na-Y and their imprisoned complexes.

Compound	Internal vibrations		External vibrations			$\nu_{(C=N)}$	$\nu_{(O-H)}$
	ν_{asym}T-O	ν_{sym}T-O	ν_{sym}T-O	ν_{asym}T-O	D-R		
Na-Y	1090	795	810	1180	610	-	3450
[VO(HNIMMPP)(H_2O)]-Y	1090	785	795	1175	550	1640	3440
[Mn(HNIMMPP)(H_2O)$_3$]-Y	1085	780	810	1181	560	1650	3450
[Fe(HNIMMPP)(H_2O)$_3$]-Y	1090	786	810	1183	550	1640	3445
[Co(HNIMMPP)(H_2O)]-Y	1090	790	815	1177	550	1640	3442
[Ni(HNIMMPP)(H_2O)]-Y	1080	789	805	1180	560	1630	3444
[Cu(HNIMMPP)(H_2O)]-Y	1090	784	800	1175	600	1630	3450

Table 4 Electronic spectroscopic data of zeolite-Y imprisoned transition metal complexes.

Compound	Wavelength (nm)	Compound	Wavelength (nm)
HNIMMPP	223, 255, 298, 347	**[VO(HNIMMPP)(H_2O)]-Y**	194, 202, 211, 306, 418
[VO(HNIMMPP)(H_2O)]	246, 206, 368	**[Mn(HNIMMPP)(H_2O)$_3$]-Y**	203, 242, 306, 316
[Mn(HNIMMPP)(H_2O)$_3$]	254, 287, 349, 386	**[Fe(HNIMMPP)(H_2O)$_3$]-Y**	193, 230, 306, 403
[Fe(HNIMMPP)(H_2O)$_3$]	212, 245, 396	**[Co(HNIMMPP)(H_2O)]-Y**	194, 241, 386, 421
[Co(HNIMMPP)(H_2O)]	218, 243, 250, 390	**[Ni(HNIMMPP)(H_2O)]-Y**	192, 202, 237, 306, 406
[Ni(HNIMMPP)(H_2O)]	199, 252, 307, 403, 438	**[Cu(HNIMMPP)(H_2O)]-Y**	194, 221, 306, 366, 402
[Cu(HNIMMPP)(H_2O)]	213, 246, 409, 497	-	-

Table 5 Oxidative reaction of styrene with TBHP as oxidant catalyzed by [VO(HNIMMPP)(H_2O)]-Y.

Catalyst	Conversion %	TOF h^{-1}	Selectivity %				
			Benzaldehyde %	Styrene oxide %	Styrene glycol %	Other polymers %	Chalcone %
[VO(HNIMMPP)(H_2O)]-Y	93.35	114.75	45.70	8.80	15.73	25.71	4.06
[Mn(HNIMMPP)(H_2O)$_3$]-Y	51.06	74.35	42.12	11.23	16.43	26.13	4.09
[Fe(HNIMMPP)(H_2O)$_3$]-Y	60.94	80.89	49.31	8.23	17.25	21.06	4.15
[Co(HNIMMPP)(H_2O)]-Y	82.34	92.55	47.32	5.23	14.02	29.45	3.98
[Ni(HNIMMPP)(H_2O)]-Y	90.43	83.37	51.39	1.37	18.34	24.64	4.26
[Cu(HNIMMPP)(H_2O)]-Y	88.03	93.31	57.18	1.49	12.04	25.33	3.96

Reaction condition: 30 mmol styrene, 60 mmol of TBHP, 10 mL acetonitrile, 0.07 g catalyst, 80°C, 10 h.

Table 6 Oxidative reaction of styrene with TBHP as oxidant catalyzed by Na-Y, VO-Y, [VO(HNIMMPP)(H_2O)], [VO(HNIMMPP)(H_2O)]-Y.

Catalyst	Conversion %	TOF	Selectivity %				
			Benzaldehyde %	Oxirane %	Styrene glycol %	Other polymers %	Chalcone %
Na-Y	3.75	-	91.24	0	2.48	6.28	0
VO-Y	76.42	93.95	90.25	0	3.86	5.89	0
[VO(HNIMMPP)(H_2O)]	88.14	14.65	43.94	8.26	14.93	26.79	6.08
[VO(HNIMMPP)(H_2O)]-Y	93.35	114.75	45.70	8.80	15.73	25.71	4.06
[VO(HNIMMPP)(H_2O)]--Y[a]	88.53	108.84	44.61	8.43	15.47	26.91	4.58
[VO(HNIMMPP)(H_2O)]--Y[b]	82.21	101.07	41.33	12.59	14.37	29.34	2.37

Reaction condition: 30 mmol styrene, 60 mmol of TBHP, 10 mL acetonitrile, 0.07 g [VO(HNIMMPP)(H_2O)]-Y catalyst, 80 °C, 10 h.